Spreading of a mycobacterial cell surface lipid into host epithelial membranes promotes infectivity

C.J. Cambier[1], Steven M. Banik[1], Joseph A. Buonomo[1], and Carolyn R. Bertozzi[1,2,*]

[1]Department of Chemistry, Stanford University, Stanford, CA, 94305, USA
[2]Howard Hughes Medical Institute, Stanford University, Stanford, CA, 94305, USA
[*]Correspondence: bertozzi@stanford.edu

ABSTRACT

Several virulence lipids populate the outer cell wall of pathogenic mycobacteria (Jackson, 2014). Phthiocerol dimycocerosate (PDIM), one of the most abundant outer membrane lipids (Anderson, 1929), plays important roles in both defending against host antimicrobial programs (Camacho et al., 2001; Cox et al., 1999; Murry et al., 2009) and in evading these programs altogether (Cambier et al., 2014a; Rousseau et al., 2004). Immediately following infection, mycobacteria rely on PDIM to evade toll-like receptor (TLR)-dependent recruitment of bactericidal monocytes which can clear infection (Cambier et al., 2014b). To circumvent the limitations in using genetics to understand virulence lipid function, we developed a chemical approach to introduce a clickable, semi-synthetic PDIM onto the cell wall of *Mycobacterium marinum*. Upon infection of zebrafish, we found that PDIM rapidly spreads into host epithelial membranes, and that this spreading inhibits TLR activation. PDIM's ability to spread into epithelial membranes correlated with its enhanced fluidity afforded by its methyl-branched mycocerosic acids. Additionally, PDIM's affinity for cholesterol promoted its occupation of epithelial membranes; treatment of zebrafish with statins, cholesterol synthesis inhibitors, decreased spreading and provided protection from infection. This work establishes that interactions between host and pathogen lipids influence mycobacterial infectivity and suggests the use of statins as tuberculosis preventive therapy by inhibiting PDIM spread.

INTRODUCTION

Mycobacterium tuberculosis, the causative pathogen of the pulmonary disease tuberculosis (TB), is estimated to have evolved within the confines of the human lung for

32 millennia (Comas et al., 2013). A result of this co-evolution is a choreographed response of
33 innate and adaptive immune cells culminating in the formation of granulomas, specialized
34 structures that permit bacterial replication and ultimately promote transmission (Ramakrishnan,
35 2012). A key strategy used by mycobacteria throughout infection is to avoid and manipulate host
36 immune pathways so as to afford the pathogen safe harbor in otherwise bactericidal myeloid
37 cells (Cambier et al., 2014a; Urdahl, 2014).
38 To better understand these host-pathogen interactions, we have taken advantage of the
39 optically transparent zebrafish larva, a natural host of the pathogen *M. marinum* (Ramakrishnan,
40 2020; Takaki et al., 2013). Infection of the hindbrain ventricle (HBV), an epithelium-lined
41 cavity, allows for the visualization and characterization of the cellular immune response (Davis
42 and Ramakrishnan, 2009), a response that is comparable to that seen in the mouse lung following
43 infection with *M. tuberculosis* (Srivastava et al., 2014). In both models, mycobacteria are
44 initially phagocytosed by tissue-resident macrophages and are eventually transferred to
45 monocytes which go on to form granulomas (Cambier et al., 2017; Cohen et al., 2018).
46 In order to reach growth-permissive cells, mycobacteria must first evade prototypical
47 anti-bacterial monocytes. In response to mucosal commensal pathogens, bactericidal monocytes
48 are recruited downstream of TLR signaling (Medzhitov, 2007). Screening of *M. marinum* genetic
49 mutants found that the cell surface lipid phthiocerol dimycocerosate (PDIM) is required to avoid
50 this TLR-dependent immune response (Cambier et al., 2014b). In addition to evading immune
51 detection, PDIM is reported to promote pathogenesis in other ways, such as being required for
52 the relative impermeability of the mycobacterial cell wall (Camacho et al., 2001) and promoting
53 escape from phagolysosomes (Augenstreich et al., 2017; Barczak et al., 2017; Lerner et al., 2017;
54 Quigley et al., 2017). However, the molecular details underlying PDIM's myriad pathogenic
55 functions remain unknown.
56 To accomplish mechanistic studies of virulence lipids, we and others developed
57 metabolic labeling strategies where unnatural metabolic precursors are fed to growing bacteria
58 (Siegrist et al., 2015). The unnatural metabolite contains a bioorthogonal functional group that
59 facilitates visualization of macromolecules in living bacteria (Sletten and Bertozzi, 2009). An
60 example is the labeling of trehalose containing lipids with azide-functionalized trehalose (Swarts
61 et al., 2012). Trehalose labeling is so robust that it has since been elaborated on with various
62 functional probes (Kamariza et al., 2018; Rodriguez-Rivera et al., 2017).

63 Here we have developed comparable chemical tools to monitor PDIM's distribution
64 during infection, allowing us to better understand PDIM's mechanism of action. By visualizing
65 PDIM during in vivo infection, we found that the first step in PDIM mediated pathogenesis is to
66 spread into epithelial cells in order to inhibit TLR signaling. Structure function analysis revealed
67 that PDIM's inherent fluidity, afforded by its methyl-branched fatty acids, promoted occupation
68 of this host lipid niche. PDIM spreading was also dependent on the lipid content of host
69 membranes. Administration of the cholesterol lowering drug, atorvastatin (Lipitor), led to a
70 decrease in PDIM spreading, and subsequent resistance to mycobacterial infection. Our findings
71 provide a mechanistic explanation for the association of statin use with a decrease in TB
72 incidence (Lai et al., 2016a) and support their use as a TB preventative therapy.
73
74 **RESULTS**
75 **Controlling Mycomembrane Composition by Chemical Extraction and Reconstitution**
76 Due to the conserved synthesis of lipid intermediates, PDIM lacks unique biosynthetic
77 precursors to facilitate metabolic labeling (Onwueme et al., 2005). However, PDIM is removed
78 following petroleum ether extraction (Moliva et al., 2019), a technique previously used to
79 perform loss of function studies of outer mycomembrane lipids (Silva et al., 1985), as lipids can
80 be removed and added back with petroleum ether (Indrigo, 2003). Using this approach, we
81 hypothesized that we could chemically install a biorthogonal handle onto extracted PDIM and
82 use this modified lipid to elucidate the fundamental mechanisms underlying PDIM's contribution
83 to virulence. Similar to reports on *M. tuberculosis* and *M. bovis,* we validated that petroleum
84 ether extraction did not affect the growth rate of *M. marinum* in culture (Supplemental Figure
85 1A) and extracted lipids could be mixed with bacteria in petroleum ether followed by drying to
86 reconstitute these lipids into the mycomembrane (Figure 1A and Supplemental Figure 1B).
87 Similar to reports in macrophages (Indrigo, 2003), following infection of zebrafish (Figure 1B)
88 delipidated bacteria were attenuated for growth and this phenotype was rescued upon
89 reconstitution (Figure 1C and D).
90
91 **Pre-infection PDIM Reservoirs are Required for Virulence**
92 *M. marinum* mutants in PDIM synthesis (Δ*mas*) and localization to the mycomembrane
93 (Δ*mmpL7*) trigger TLR-dependent immune recognition following infection (Cambier et al.,

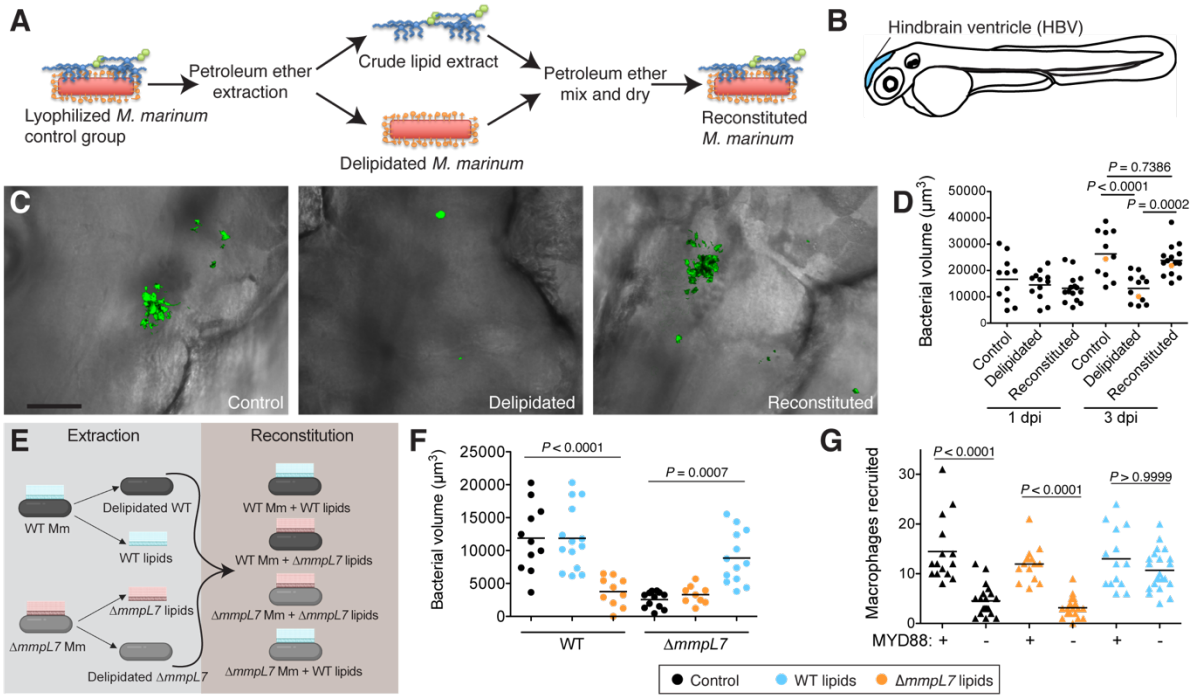

Figure 1. Chemical extraction and reconstitution reveals that pre-infection PDIM reservoirs are required for virulence. (**A**) Model of chemical extraction and reconstitution. (**B**) Model of zebrafish larva showing the hindbrain ventricle (HBV) injection site. (**C**) Representative images of the experiment in **D** (orange dots), scale bar = 50μm. (**D**) Mean bacterial volume after HBV infection of wildtype fish with ~100 control, delipidated, or reconstituted *M. marinum*. (**E**) Model of lipid swap experiment. (**F**) Mean bacterial volume after HBV infection of wildtype fish with ~100 WT or Δ*mmpL7 M. marinum* treated as follows: non-extracted control (black), extracted and reconstituted with WT lipids (blue), or extracted and reconstituted with Δ*mmpL7* lipids (orange). (**G**) Mean macrophage recruitment at 3 hpi of the HBV with ~100 Δ*mmpL7 M. marinum* as treated in **F**. (**D**), (**F**), and (**G**) representative of at least three separate experiments. Ordinary one-way ANOVA with (**D**) Sidak's multiple comparisons test for the comparison's shown and (**F**) Tukey's multiple comparisons test with selected adjusted *P* values shown. (**G**) Kruskal-Wallis ANOVA for unequal variances with Dunn's multiple comparisons test with selected adjusted *P* values shown.

2014b). TLR signaling leads to the recruitment of activated monocytes that can clear bacteria in an inducible nitric oxide synthase-dependent fashion. PDIM-sufficient wildtype bacteria are not detected by TLRs and instead recruit a comparable number of permissive monocytes downstream of the chemokine CCL2 (Cambier et al., 2014b). However, since Δ*mas* and Δ*mmpL7* lack proteins required for PDIM's synthesis or export, the associated phenotypes could be attributed to the missing proteins rather than to a lack of PDIM. To directly test if the presence of PDIM on the bacterial surface is responsible for evasion of TLR-mediated immunity, we performed a lipid-swap experiment. Wildtype and Δ*mmpL7 M. marinum* were either untreated (control) or extracted and reconstituted with their native lipids or the lipids from the other strain (Figure 1E). Petroleum ether extraction of wildtype bacteria completely removed both dimycocerosic acid (DIM) containing lipids, PDIM and its metabolic precursor

106 phthiodiolone dimycocerosate (PNDIM, Supplemental Figure 1C) both of which were absent in
107 Δ*mmpL7* extracts (Supplemental Figure 1D). Following infection, wildtype control and wildtype
108 bacteria reconstituted with wildtype lipids grew normally whereas wildtype bacteria
109 reconstituted with Δ*mmpL7* lipids were attenuated for growth (Figure 1F). Conversely, Δ*mmpL7*
110 bacteria were attenuated for growth, as expected, unless they were reconstituted with wildtype
111 lipids, in which case they grew at wildtype bacterial rates (Figure 1F). Using an antisense
112 morpholino to knockdown the TLR-adaptor MYD88 (Bates et al., 2007), we also found that the
113 dependence on TLRs to recruit monocytes to Δ*mmpL7* bacteria was abolished with wildtype
114 lipids (Figure 1G). Taken together these experiments highlight the strengths of this chemical
115 approach. Not only does it recapitulate known phenotypes of PDIM genetic mutants, but it
116 directly links the mutant phenotypes to the absence of PDIM on the mycomembrane.
117 Furthermore, our data suggest that the PDIM present on the surface of the bacterium from the
118 onset of infection is required and sufficient to avoid TLRs, as mutants unable to replenish PDIM
119 on their surfaces become virulent when they are coated with wildtype lipids prior to infection.
120

121 **Synthesis of a Clickable, Biologically Active PDIM**

122 Given the pathogenic importance of the pre-infection mycomembrane lipid content, we
123 hypothesized that labeling this pool of PDIM would allow us to observe characteristics
124 underlying its virulence mechanisms. Both PDIM and its biosynthetic precursor PNDIM are
125 present in the outer mycomembrane. The only difference between these lipids is their diol
126 backbones; PDIM has a methyl ether, while PNDIM has a ketone (Siméone et al., 2007). Either
127 lipid alone can promote infection in mice (Siméone et al., 2007), suggesting chemical flexibility
128 at this site with regards to virulence. Therefore, we converted the methyl ether of PDIM to an
129 alkyl halide with trimethylsilyl iodide (Jung and Lyster, 1977). Subsequent addition of sodium
130 azide provided azido-DIM (Figure 2A). Reconstitution of delipidated bacteria with lipids
131 containing azido-DIM, followed by a copper-free click reaction with the cyclooctyne fluorophore
132 DIBO-488 (Figure 2B) resulted in a ~100-fold increase in fluorescence (Figure 2C). Confocal
133 microscopy revealed the fluorescent signal to be membrane associated (Figure 2D, E),
134 suggesting azido-DIM incorporated into the mycomembrane. Importantly, we found that adding
135 back native DIMs or azido-DIM to DIM-depleted lipids prior to reconstitution (Supplemental
136 Figure 1E) followed by DIBO-488 labeling rescued DIM-depleted bacteria's growth attenuation

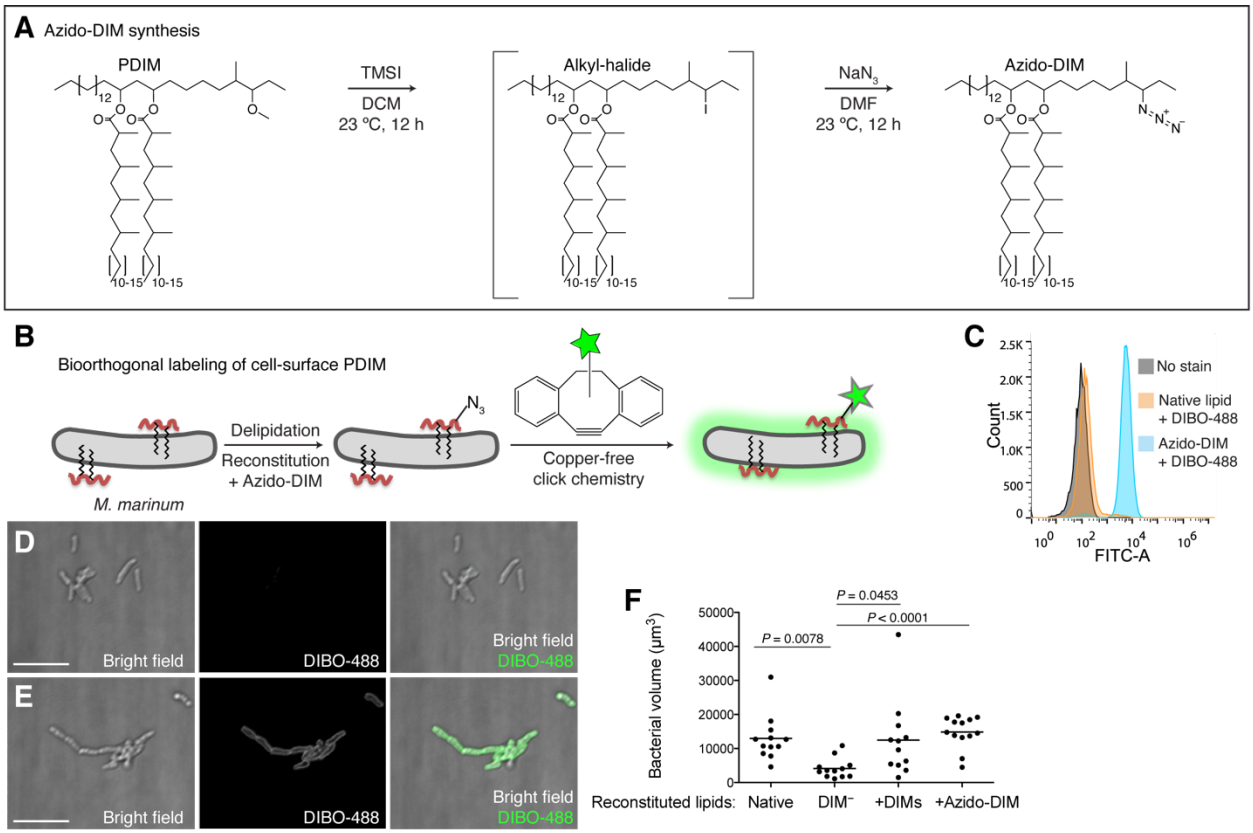

Figure 2. Synthesis and application of a chemically tractable, biologically active PDIM variant, azido-DIM. (**A**) Synthesis of azido-DIM. (**B**) Model of delipidation and reconstitution of bacteria with or without azido-DIM followed by treatment with an azide-reactive cyclooctyne, DIBO-488. (**C**) Flow cytometry analysis of control or azido-DIM reconstituted bacteria treated or untreated with DIBO-488. Image of (**D**) control or (**E**) azido-DIM reconstituted bacteria treated with DIBO-488, scale bar = 8μm. (**F**) Mean bacterial volume 3 days following HBV infection of wildtype fish with ~100 delipidated *M. marinum* reconstituted with Native, DIM depleted (DIM$^-$), DIM$^-$ plus native DIMs (+DIMs), or DIM$^-$ plus azido-DIM (+Azido-DIM) lipids. Kruskal-Wallis ANOVA for unequal variances with Dunn's multiple comparisons test with selected adjusted *P* values shown. (**C**)-(**F**) representative of three separate experiments.

(Figure 2F). Thus, with this approach we can generate bacteria with chemically functionalized PDIM that retain their pathogenicity.

PDIM Spreads into Host Cell Membranes In Vivo

To visualize PDIM's distribution, we infected zebrafish with blue-fluorescent *M. marinum* that were reconstituted with azido-DIM followed by labeling with DIBO-488 (DIM-488). Immediately following phagocytosis, DIM-488 appeared to spread away from bacteria into host membranes (Supplemental Figure 2A). Real-time imaging revealed that the spreading was dynamic in nature, with DIM-488 deposits moving relative to host cells (Supplemental Movie 1). To better visualize spreading of PDIM, we used the transgenic zebrafish line *Tg(mfap4:tdTomato)* whose macrophages express the fluorescent protein tdTomato (Walton et

149 al., 2015). As early as 3 hours post-infection (hpi), DIM-488 had spread into infected
150 macrophage membranes, at both phagosome (Figure 3A, arrows) and more distal membrane sites
151 (Figure 3A, arrow heads). Spreading increased across macrophage membranes by 3 days post-
152 infection (dpi) (Figure 3B). Similar spreading was seen when azido-DIM was conjugated to
153 DIBO-647 (Supplemental Figure 2B, C), suggesting that the lipid, and not the fluorescent probe,
154 was responsible for this phenotype. To quantify the extent of PDIM spreading, we imaged the
155 entire HBV infection site and calculated the proportion of fluorophore labelled azido-DIM that
156 no longer localized with bacteria (Supplemental Figure 2D). Using this number as a proxy for
157 lipid spread, we saw an increase in spreading as infection progressed (Figure 3C). Spreading also
158 occurred following infection of THP-1 macrophages in culture (Supplemental Figure 2E).
159 These results were consistent with a recent report using cultured macrophages showing
160 that *M. tuberculosis* PDIM occupies their cell membranes (Augenstreich et al., 2019).
161 Nevertheless, we wanted to determine whether spreading was a true attribute of our labeled
162 PDIM or if it was an artifactual property due to our reconstitution method. To address this, we
163 used an established pan-glycolipid labeling method previously used to track the spread of
164 mycobacterial glycolipids into macrophage membranes (Beatty et al., 2000). Control and
165 reconstituted *M. marinum* were treated with periodate and then reacted with a fluorescent
166 hydroxylamine prior to infection (Beatty et al., 2000). We found that spreading of the total pool
167 of fluorophore-labeled glycolipids was equal between control and reconstituted bacteria
168 (Supplemental Figure 3A and B). Thus, reconstitution does not appreciably influence the
169 spreading dynamics of mycomembrane lipids. These data demonstrate that the introduction of a
170 chemically functionalized PDIM into the mycomembrane provides physiologically relevant
171 information regarding PDIM's host distribution during in vivo infection.
172 We next wanted to understand how PDIM spreading might be promoting virulence.
173 While it is appreciated that mycobacterial lipids spread throughout macrophage membranes
174 (Beatty et al., 2000), the inability to track specific lipids in an in vivo setting has hampered
175 studies on the pathophysiological relevance of these observations. PDIM has been suggested to
176 interact with the protein substrates of the type VII secretion system ESX-1, including EsxA
177 (Barczak et al., 2017). PDIM and EsxA are both required for cytosolic escape from
178 phagolysosomes (Osman et al., 2020; Quigley et al., 2017; van der Wel et al., 2007), where
179 PDIM is suggested to enhance the pore forming activity of EsxA through its ability to infiltrate

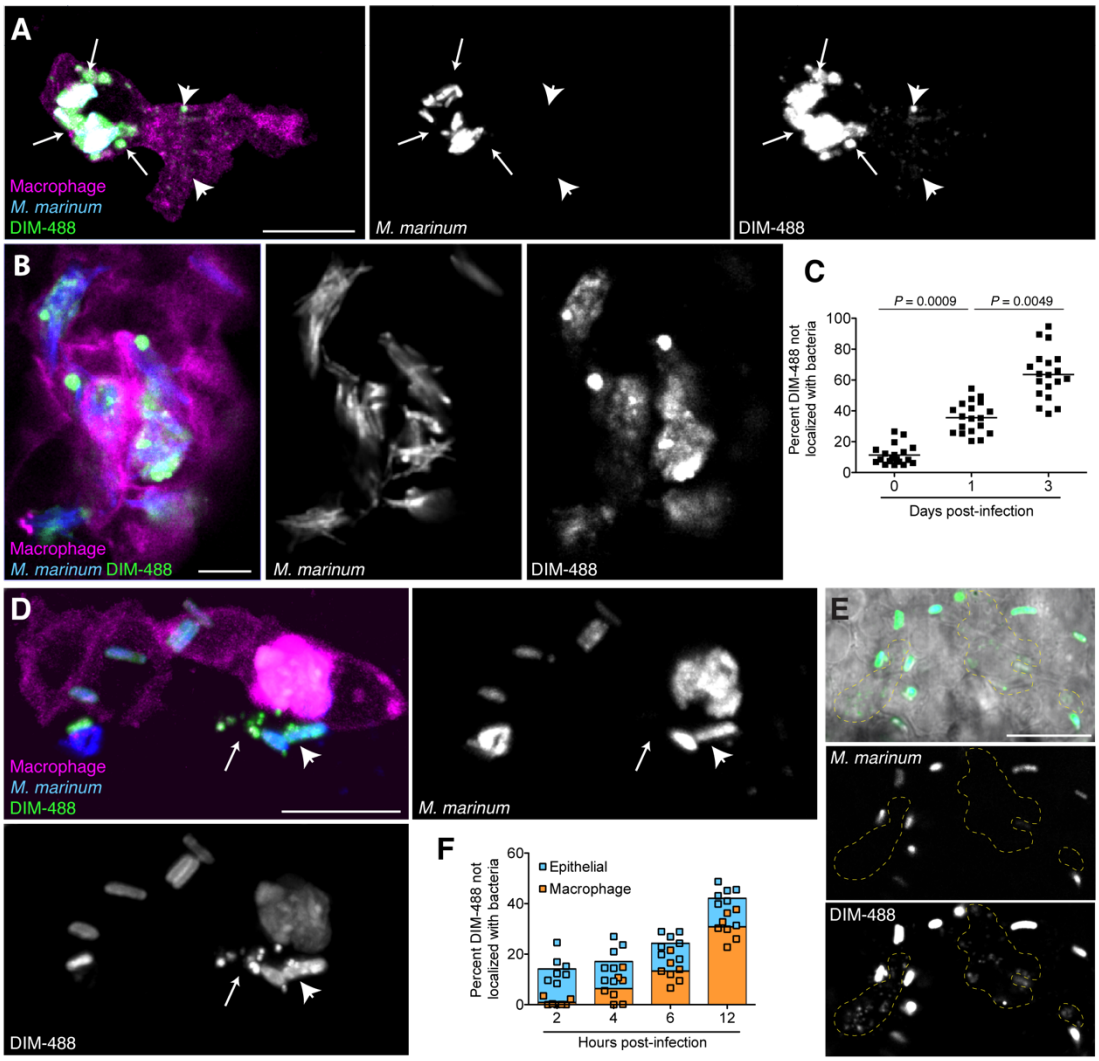

Figure 3. PDIM spreads into host cell membranes. Images of *M. marinum* expressing a cytosolic blue fluorescent protein reconstituted with DIBO-488 labeled azido-DIM (DIM-488) at (**A**) 3 hpi and (**B**) 3 dpi of ~100 *M. marinum* in the HBV of transgenic fish whose macrophages express a fluorescent protein. Scale bar = 10 µm. Arrows, DIM-488 spread in vicinity of phagosome, arrowheads, DIM-488 spread throughout macrophage. (**C**) Mean percent DIM-488 not localized with bacteria following HBV infection of wildtype fish with ~100 *M. marinum*. Kruskal-Wallis ANOVA for unequal variances with Dunn's multiple comparisons test with selected adjusted *P* values shown. Representative of at least three separate experiments. (**D**) Image highlighting DIM-488 spread from bacteria (arrowhead) to epithelial cells (arrows) at 3 hpi of ~100 *M. marinum* in the HBV, colors correspond to features defined in **A**, scale bar = 10*µ*m. (**E**) Image highlighting DIM-488 spread onto epithelial surfaces (yellow-dashed outline) at 2 hpi of ~100 *M. marinum* in the HBV, scale bar = 10*µ*m. (**F**) Mean percent DIM-488 in macrophage or epithelial cells not localized with bacteria following HBV infection with ~100 *M. marinum*. Representative of two separate experiments.

macrophage membranes (Augenstreich et al., 2017). Thus, we hypothesized that PDIM localization would be dependent on EsxA secretion. Region of difference-1 *M. marinum* mutants (ΔRD1) which lack EsxA (Volkman et al., 2010), were reconstituted with DIM-488 prior to zebrafish infection. There was no difference in DIM-488 spreading kinetics between wildtype and ΔRD1 *M. marinum* (Supplemental Figure 3C), suggesting that EsxA does not influence

186 PDIM spreading. Besides playing a role in cytosolic escape, PDIM spreading into macrophage
187 membranes has also been shown to promote phagocytosis of extracellular bacteria (Astarie-
188 Dequeker et al., 2009; Augenstreich et al., 2019). To test this in vivo, we measured the rate of
189 phagocytosis of wildtype or Δ*mmpL7 M. marinum* following HBV infection by measuring the
190 number of discrete bacterial objects over time. As bacteria are phagocytosed, individual bacteria
191 can no longer be discerned by confocal microscopy and the number of discrete objects decreases.
192 There was no measurable difference in the rate of phagocytosis of wildtype or Δ*mmpL7* bacteria
193 (Supplemental Figure 3D).
194 Given the discrepancy regarding PDIM's role in promoting phagocytosis between the
195 cultured macrophage and zebrafish models, we wondered if the activation state of responding
196 monocyte/macrophage populations in zebrafish larvae was influencing their phagocytic
197 capacities. We know that PDIM-deficient bacteria recruit antimicrobial monocytes downstream
198 of TLR signaling, whereas wildtype bacteria recruit permissive monocytes downstream of
199 CCL2/CCR2 signaling (Cambier et al., 2014b). We also know that wildtype bacteria depend on
200 resident macrophages to produce CCL2 in order to recruit CCR2-expressing monocytes, whereas
201 PDIM-deficient bacteria recruit monocytes independent of resident macrophages (Cambier et al.,
202 2017). Therefore, we wondered if PDIM plays a critical role in evading TLR detection in non-
203 macrophage cell populations prior to any of its documented roles in directly modulating
204 macrophage biology. Upon closer examination, we observed DIM-488 deposits on zebrafish
205 epithelium at 24 hpi (Supplemental Figure 3E, arrows). Imaging at 3 hpi we captured
206 extracellular bacteria having spread DIM-488 in the vicinity of an infected macrophage (Figure
207 3D). This ability to spread into epithelial membranes was confirmed in human A549 epithelial
208 cells in vitro (Supplemental Figure 3F). To address the timing of PDIM spread into epithelial and
209 macrophage membranes we imaged infected zebrafish at 2 hpi, prior to macrophage
210 phagocytosis, and at 4, 6, and 12 hpi by which time the majority of bacteria are phagocytosed.
211 Preceding any appreciable spreading onto macrophages, DIM-488 had already spread onto
212 epithelial cells by 2 hpi (Figure 3E yellow outlines and 3F). These data suggest that
213 mycobacteria spread PDIM onto epithelial cells prior to interactions with macrophages. To
214 confirm this observation, we depleted macrophages from zebrafish larva using clodronate-loaded
215 liposomes (Bernut et al., 2014). DIM-488 spreading still occurred in the absence of macrophages

216 (Supplemental Figure 3G). These data demonstrate that PDIM spreads onto epithelial cells
217 independent of and prior to macrophage phagocytosis.
218
219 **PDIM's Fluidity Promotes Spread into Epithelial Cell Membranes**
220 We sought to understand PDIM's properties that facilitated its ability to spread into host
221 membranes. It is well established that increased membrane fluidity promotes membrane mixing
222 (Howell et al., 1972), leading us to ask if PDIM occupied membrane domains of high fluidity.
223 Previous studies from our lab found that the mycomembrane of *Mycobacterium smegmatis* is
224 relatively immobile by using fluorescence recovery after photobleaching (FRAP) of
225 metabolically labeled trehalose monomycolate (TMM) (Rodriguez-Rivera et al., 2017). We
226 confirmed this for *M. marinum* TMM. Using the metabolic label 6-azido-trehalose (Swarts et al.,
227 2012) followed by reaction with DIBO-488 to track TMM (TMM-488), we found very little
228 recovery following photobleaching of TMM-488, with only around 40% of the labeled lipids
229 being mobile (Figure 4A–C, and Supplemental Figure 4A). When we assessed PDIM, we found
230 DIM-488 recovery to be very efficient, with a half-life of 3 seconds and around 95% of the
231 signal being mobile (Figure 4A–C, and Supplemental Figure 4B). Thus, PDIM-containing
232 mycomembrane domains have a uniquely high fluidity.
233 If high membrane fluidity facilitates membrane mixing, then TMM should not be able to
234 spread into host cells as efficiently as PDIM does. Indeed, we found that TMM-488 failed to
235 spread onto epithelial cells at 2 hpi. Only when phagocytosed within macrophages at 24 hpi was
236 TMM spreading detected (Figure 4D and Supplemental Figure 4C). Even in the absence of
237 macrophages, where bacteria have a prolonged contact time with epithelial cells, TMM-488
238 spreading was negligible (Figure 4E). Thus, mycomembrane fluidity appears to correlate with
239 the ability to spread into host epithelial membranes.
240 To determine if there is a causal relationship between fluidity and spreading, we used
241 FRAP to identify conditions that decreased PDIM's recovery after photobleaching. Neither heat-
242 killing nor mild chemical fixation (4% paraformaldehyde (PFA)) significantly reduced DIM-
243 488's recovery (Figure 4F, G and Supplemental Figure 5). However, fixation with 4% PFA + 1%
244 glutaraldehyde (GA), a more effective fixative for membrane-associated proteins (Huebinger et
245 al., 2018), resulted in an almost 80% reduction in the mobile fraction of DIM-488 (Figure 4F, G
246 and Supplemental Figure 5). PFA+GA treatment decreased DIM-488 spread onto epithelial cells

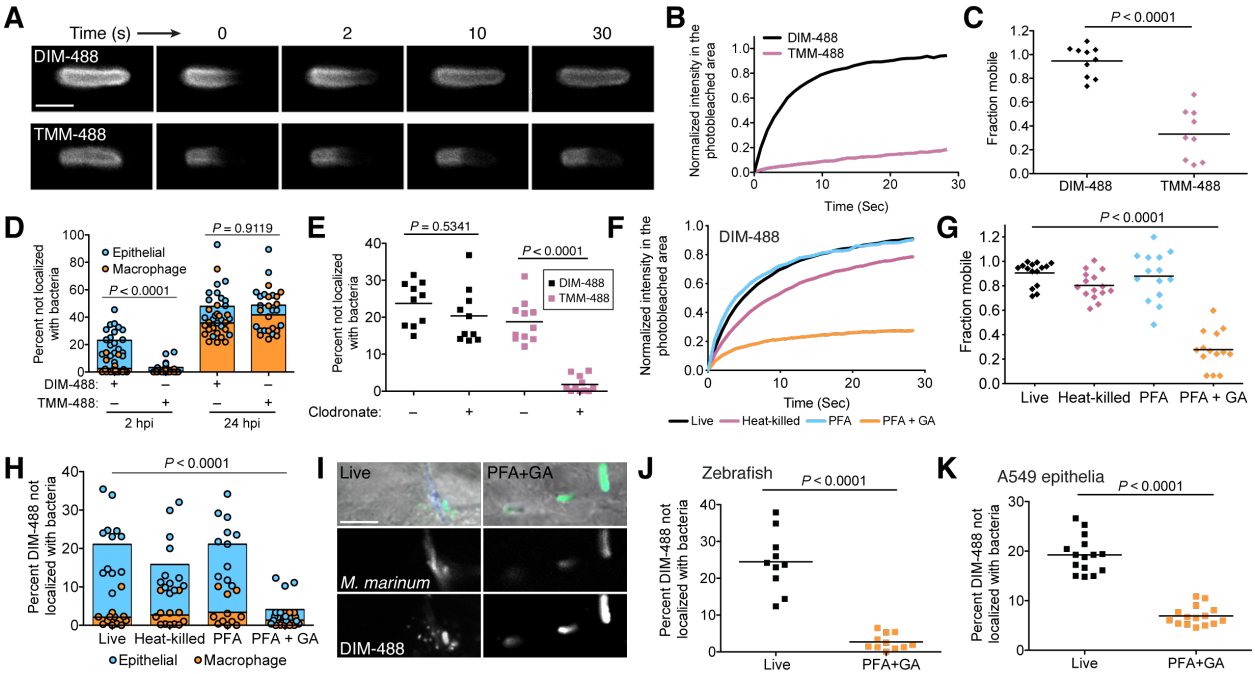

Figure 4. PDIM's mobility promotes spread into epithelial cells. (**A**) Representative FRAP images of DIM-488 and TMM-488 labeled *M. marinum*, scale bar = 2μm. (**B**) Fluorescent recovery curves after photobleaching of DIM-488 or TMM-488 labeled *M. marinum*, lines represent the average signal from n = 10 cells. (**C**) Mean fraction mobile following fitting of FRAP curves to data generated in **B**. (**D**) Mean percent DIM-488 or TMM-488 in macrophage or epithelial cells not localized with bacteria following HBV infection with ~100 *M. marinum,* two-tailed Mann whitney test. (**E**) Mean percent DIM-488 or TMM-488 not localized with bacteria 24 h following HBV infection of lipo-PBS or lipo-clodronate treated fish with ~100 *M. marinum*. (**F**) Fluorescent recovery curves after photobleaching of live, heat-killed, 4% paraformaldehyde (PFA) fixed, or 4% paraformaldehyde plus 1% glutaraldehyde (PFA+GA) fixed DIM-488 labeled *M. marinum*, lines represent the average signal from n = 14-15 cells. (**G**) Mean fraction mobile following fitting of FRAP curves to data generated in **F**. (**H**) Mean percent DIM-488 in macrophage or epithelial cells not localized with bacteria 2 h following HBV infection with ~100 *M. marinum* treated as in **F**. (**I**) Images of live or PFA+GA treated DIM-488 labeled *M. marinum* at 2 hpi of the HBV with ~100 bacteria, scale bar = 5μm. Mean percent DIM-488 not localized with bacteria 24 h following (**J**) infection of lipo-clodronate treated fish or (**K**) A549 epithelial cells with live or PFA+GA fixed DIM-488 labeled *M. marinum*. (**C**), (**J**), and (**K**) two-tailed, unpaired t test. (**E**), (**G**), and (**H**) ordinary one-way ANOVA with Tukey's multiple comparisons test with selected adjusted *P* values shown. (**B**)-(**H**) and (**J**)-(**K**) representative of three separate experiments.

at 2 hpi (Figure 4H and 4I). Likewise, fixed DIM-488 did not spread into epithelial membranes following a 24 h infection of macrophage-depleted zebrafish (Figure 4J). Nor did it spread onto A549 epithelial cells after 24 h (Figure 4K). Together these results suggest that PDIM's fluidity promotes spreading into epithelial membranes.

PDIM's Methyl-Branched Mycocerosic Acids Promote Fluidity and Spreading

To further test if PDIM's high membrane fluidity is responsible for its spreading, we sought to take advantage of our ability to alter PDIM's structure. Lipid structure is known to modulate membrane fluidity (Los and Murata, 2004). Saturated lipids form closely packed

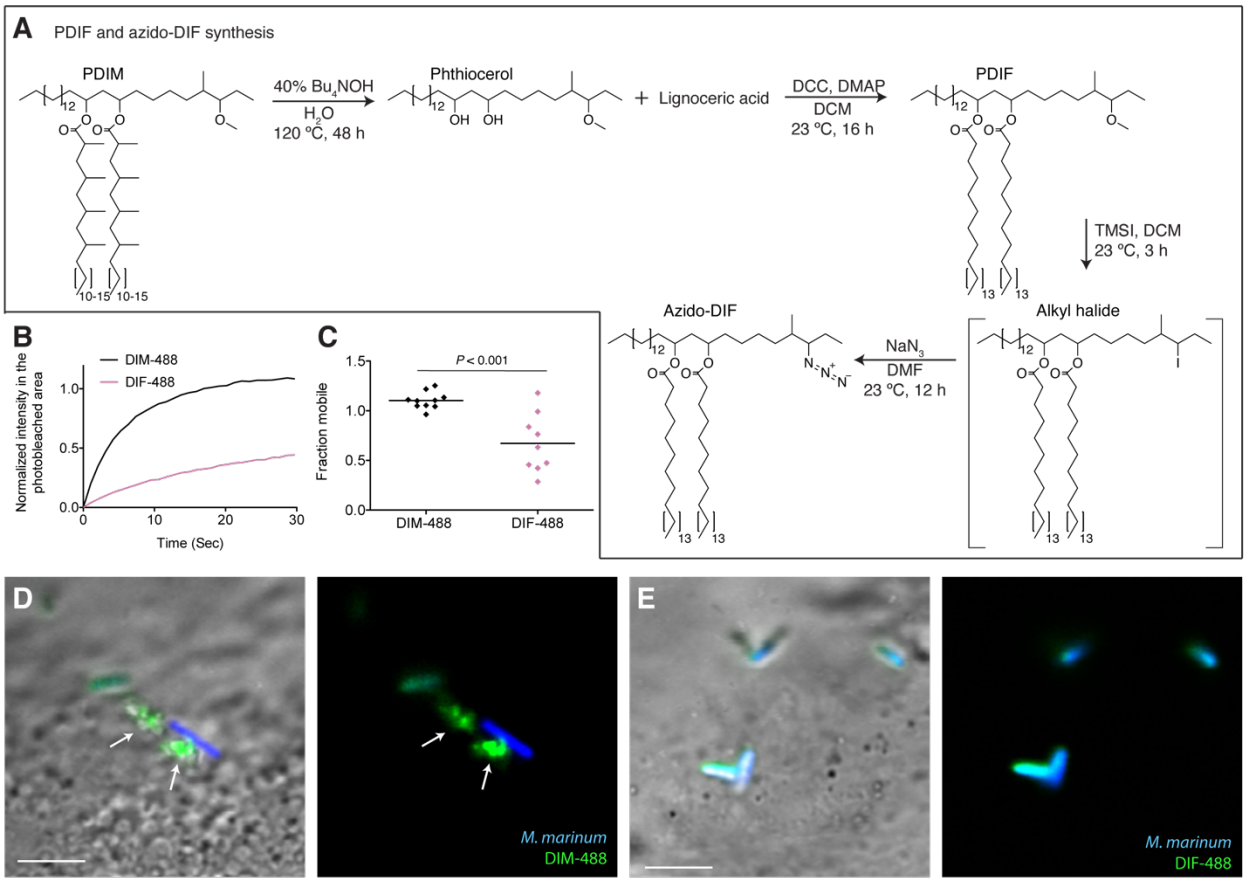

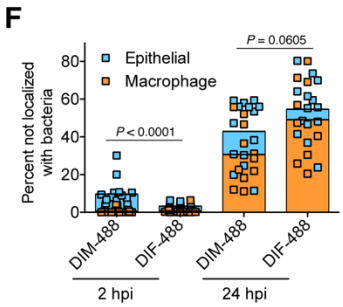

Figure 5. PDIM's methyl-branched mycocerosic acids are required for virulence. (**A**) Phthiocerol di-fatty acid (PDIF) and azido-DIF synthesis. (**B**) Fluorescent recovery curves after photobleaching of DIM-488 or DIF-488 labeled *M. marinum*, lines represent the average signal from n = 9-10 cells. (**C**) Fraction mobile following fitting of FRAP curves to data generated in **B**. Two-tailed, unpaired t test. Images of *M. marinum* expressing a blue fluorescent protein reconstituted with (**D**) DIM-488 or (**E**) DIF-488 at 2 hpi into the HBV of wildtype fish, arrows indicated spread signal, scale bar = 5μm. (**F**) Mean percent DIM-488 or DIF-488 in macrophage or epithelial cells no longer localized with bacteria following HBV infection with ~100 *M. marinum*. Two-tailed Mann Whitney test for 2 hpi and two-tailed, unpaired t test for 24 hpi. (**B**), (**C**), and (**F**) Representative of three separate experiments.

assemblies giving rise to more rigid bilayers, while unsaturated lipids do not pack as tightly and produce more fluid bilayers. Methyl branches on otherwise saturated lipids have also been shown to increase membrane fluidity (Budin et al., 2018; Poger et al., 2014). Therefore, we hypothesized that PDIM's methyl-branched mycocerosic acids determine its fluidity. To test this, we hydrolyzed PDIM with tetrabutylammonium hydroxide to isolate phthiocerol. We then esterified phthiocerol with the saturated fatty acid lignoceric acid that resulted in straight chain lipids of comparable length to mycocerosic acid. This phthiocerol di-fatty acid (PDIF) was then treated similarly to PDIM (Figure 2A) to yield the azide-labeled PDIF, azido-DIF (Figure 5A).

266 FRAP studies confirmed that DIBO-488 labeled azido-DIF (DIF-488) was not as mobile as
267 DIM-488, with only ~50% in the mobile fraction (Figure 5B, C and Supplemental Figure 6A–C).
268 Upon zebrafish infection, DIF-488 failed to spread onto epithelial cells at 2 hpi (Figure 5D–F).
269 However, similar to other mycobacterial lipids (Beatty et al., 2000) including TMM (Figure 4A),
270 DIF-488 was capable of spreading into macrophage membranes at later timepoints (Figure 5F
271 and Supplemental Figure 6D, E). Thus, PDIM's high fluidity mediated by its methyl-branched
272 lipid tails is the reason for its unique ability to spread into epithelial membranes.
273
274 **PDIM Spreading into Epithelial Membranes is Required to Evade TLRs**
275 Is PDIM spreading into epithelial membranes required to inhibit TLR signaling? We first
276 evaluated monocyte recruitment towards infecting mycobacteria to address this question.
277 Wildtype *M. marinum* must be alive in order to stimulate resident macrophages to express CCL2
278 to recruit permissive monocytes as heat-killed bacteria failed to do so (Cambier et al., 2017). In
279 contrast, PDIM-deficient *M. marinum* do not depend on resident macrophages to recruit
280 bactericidal monocytes and do so in a manner independent of bacterial viability (Cambier et al.,
281 2017). We now wondered if, in order for mycobacteria to gain access to resident macrophages,
282 PDIM must first spread into epithelial membranes to prevent recruitment of bactericidal
283 monocytes. We confirmed that heat-killed mycobacteria do not recruit monocytes (Figure 6A).
284 Likewise, PFA-treated bacteria which can also spread PDIM did not recruit monocytes (Figure
285 6A). However, monocyte recruitment towards PFA+GA treated bacteria, which do not spread
286 PDIM, phenocopied heat-killed Δ*mmpL7 M. marinum*; even though they are not viable, they
287 recruited monocytes to a similar extent as live bacteria (Figure 6A). Moreover, this monocyte
288 recruitment was now downstream of TLR signaling, as knockdown of MYD88 prevented
289 monocyte recruitment towards PFA+GA treated bacteria (Figure 6B). Taken together these data
290 demonstrate that PDIM spreading into epithelial membranes is required to prevent TLR-
291 dependent recruitment of monocytes.
292 TLR signaling has been shown to recruit microbicidal monocytes that kill infecting
293 bacteria (Cambier et al., 2014b). Not only are PDIM-deficient bacteria killed but co-infected
294 PDIM-expressing bacteria are as well (Cambier et al., 2014b). This latter finding allowed us to
295 directly examine the link between PDIM spreading and bacterial killing by resultant TLR-
296 signaled monocytes. We infected larvae with live red-fluorescent wildtype *M. marinum* along

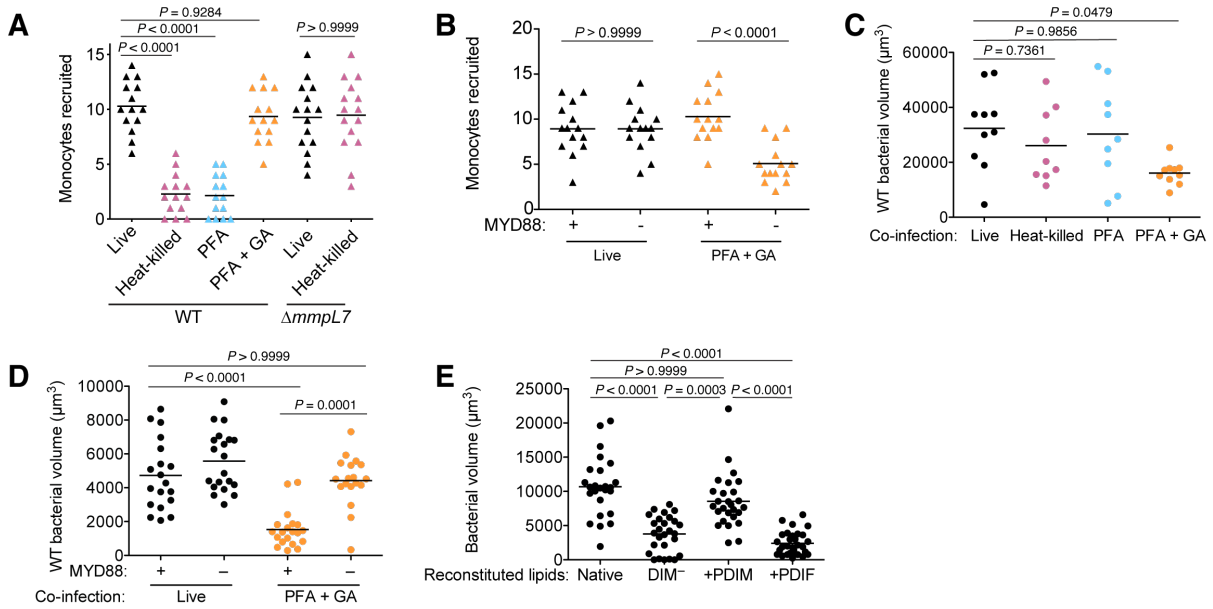

Figure 5. PDIM spreading into epithelial membranes is required to evade TLRs. (**A**) Mean monocyte recruitment at 3 hpi of the HBV with ~100 live, heat-killed, PFA treated, or PFA+GA treated wildtype (WT) or ~100 live or heat-killed Δ*mmpL7 M. marinum*. (**B**) Mean monocyte recruitment at 3 hpi of the HBV of wildtype or MYD88-depleted fish with ~100 live or PFA+GA treated wildtype *M. marinum*. Mean volume of wildtype *M. marinum* following co-infection with (**C**) wildtype *M. marinum* treated as in **A** or (**D**) live or PFA+GA treated wildtype *M. marinum* in wildtype or MYD88-depleted fish. (**E**) Mean bacterial volume 3 days following HBV infection of wildtype fish with ~100 *M. marinum* reconstituted with Native, DIM-depleted (DIM⁻), DIM⁻ plus PDIM (+PDIM), or DIM⁻ plus PDIF (+PDIF) lipids. (**A**)-(**C**) ordinary one-way ANOVA with Tukey's multiple comparisons test with selected adjusted *P* values shown. (**D**) and (**E**) Kruskal-Wallis ANOVA for unequal variances with Dunn's multiple comparisons test with selected adjusted *P* values shown. (**A**)-(**E**) representative of three separate experiments.

with green-fluorescent wildtype *M. marinum* that were live (untreated), heat-killed, PFA treated, or PFA+GA treated and then determined the burdens of the red fluorescent wildtype *M. marinum* at 3 dpi. Only co-infection with PFA+GA treated bacteria caused attenuation of wildtype bacteria (Figure 6C). Moreover, this attenuation was dependent on MYD88 (Figure 6D). Lastly, we asked if PDIF, which is unable to spread into epithelial cells (Figure 4F), could rescue DIM-deficient bacterial growth similarly to PDIM (Figure 2F). Consistent with the requirement for PDIM to spread into epithelial cells to promote virulence, we found that reconstitution with PDIF does not rescue bacterial growth (Figure 6E). Together these findings implicate PDIM spreading into epithelial membranes in inhibiting TLR signaling and the resultant recruitment of microbicidal monocytes that can kill infecting mycobacteria.

311 **Host Cholesterol Promotes PDIM Spread and Mycobacterial Infectivity**

312 We next asked if host lipids also influence PDIM spreading. Cholesterol has been
313 reported to modulate macrophage interactions with mycobacteria (Gatfield and Pieters, 2000).
314 However, three lines of evidence suggest a macrophage-independent relationship between
315 mycobacteria and cholesterol: 1) 36% of the lipid extracted from *Mycobacterium bovis* harvested
316 from necrotic mouse lung (where macrophages are sparse) was found to be host cholesterol
317 (Kondo and Kanai, 1976); 2) mycobacterial-associated cholesterol was isolated as a mixture with
318 PDIM (Kondo and Kanai, 1976); 3) *M. tuberculosis* grown in culture can sequester cholesterol to
319 its outer mycomembrane, a process dependent on mycomembrane lipids (Brzostek et al., 2009).
320 To test if host cholesterol interacted with PDIM to facilitate its spreading, we first grew wildtype
321 and Δ*mmpL7 M. marinum* in the presence of alkyne-cholesterol (Supplemental Figure 7A) for 48
322 h, followed by treatment with azide-conjugated alexafluor-647. We found that only wildtype *M.*
323 *marinum* could sequester cholesterol to their mycomembrane (Figure 7A–C). We next tested
324 whether cholesterol contributes to spreading of PDIM into host membranes. We depleted
325 cholesterol from A549 epithelial cells with methyl β–cyclodextrin (MßCD) which resulted in an
326 eight-fold decrease in cholesterol (Supplemental Figure 7B). This was associated with decreased
327 DIM-488 spreading (Supplemental Figure 7C). Importantly, in MßCD treated cells we could
328 restore cholesterol to untreated levels with water-soluble cholesterol, and this restored DIM-488
329 spreading (Supplemental Figure 7B, C). To test if host cholesterol facilitates PDIM spreading in
330 vivo, we treated zebrafish with statins, drugs that inhibit HMG-CoA reductase, the rate-limiting
331 step of cholesterol biosynthesis. Specifically, we used atorvastatin which was shown to lower
332 cholesterol in zebrafish (Maerz et al., 2019). Following 24 h of treatment, atorvastatin decreased
333 cholesterol levels in the larvae by 25%, and co-treatment with water-soluble cholesterol restored
334 cholesterol levels (Figure 7D). Atorvastatin treatment also decreased DIM-488 spreading onto
335 epithelial cells (Figure 7E and F), suggesting that PDIM's interaction with cholesterol promotes
336 spreading into epithelial membranes in vivo.

337 Hypercholesteremia has been shown to exacerbate mycobacterial infection in mice and
338 humans (Martens et al., 2008; Soh et al., 2016), and studies suggest the utility of statins both in
339 TB treatment and prevention. When used in mice, statins decreased the duration of TB therapy
340 by one month (Dutta et al., 2016), and studies of health care databases found that statin use is
341 associated with decreased incidence of TB (Kim et al., 2019; Lai et al., 2016b). Accordingly, we

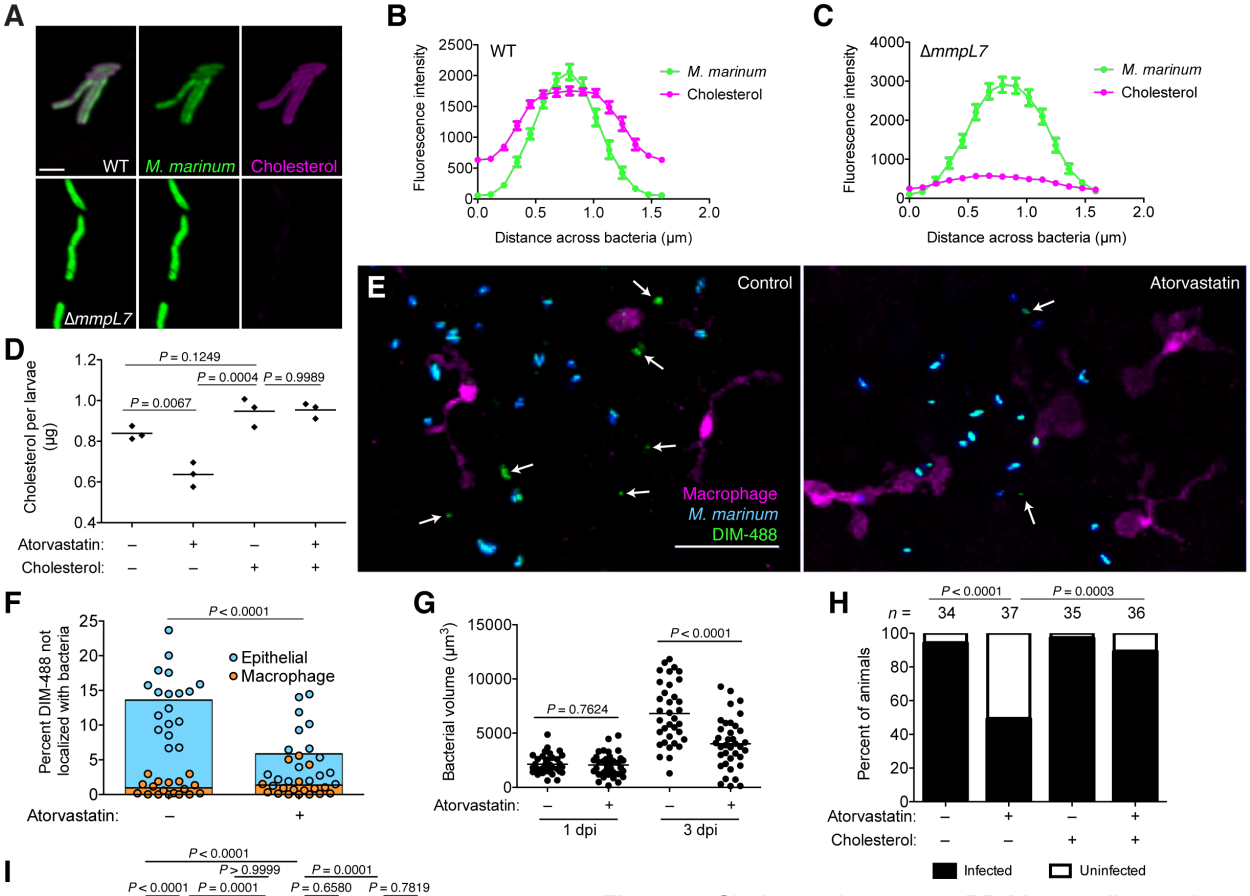

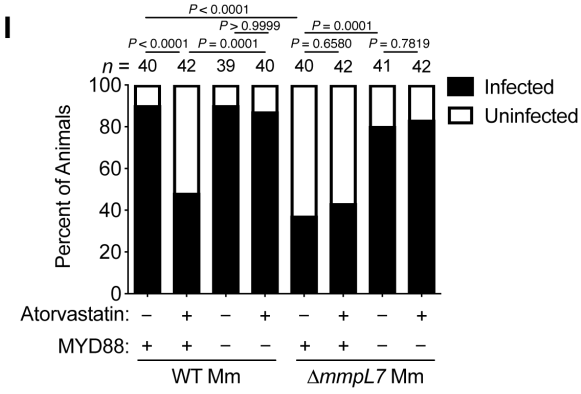

Figure 7. Cholesterol promotes PDIM spreading and mycobacterial infectivity. (**A**) Images of wildtype (WT) and Δ*mmpL7 M. marinum* expressing a green fluorescent protein following 48 h incubation with alkyne-cholesterol reacted with AlexaFlour647 Azide, scale bar = 3μm. Mean (±SEM) fluorescent intensity of line profiles drawn perpendicular to poles of (**B**) WT and (**C**) Δ*mmpL7 M. marinum* labeled as in **A**. (**D**) Mean cholesterol content of 3 dpf zebrafish following a 24 h treatment with atorvastatin, water-soluble cholesterol, or both. Ordinary one-way ANOVA with Tukey's multiple comparisons test with selected adjusted *P* values shown. (**E**) Images of control or atorvastatin treated transgenic fish whose macrophages express tdTomato at 2 hpi with ~100 *M. marinum* expressing a cytosolic blue fluorescent protein reconstituted with DIBO-488 labeled azido-DIM (DIM-488), scale bar = 40μm. Arrows, DIM-488 spread onto epithelial cells. (**F**) Mean percent DIM-488 in macrophage or epithelial cells not localized with bacteria at 2 h following HBV infection with ~100 *M. marinum* in control or atorvastatin treated fish. Two-tailed, unpaired t test. (**G**) Mean bacterial volume following HBV infection of control or atorvastatin treated fish with ~100 *M. marinum*. Two-tailed Mann Whitney test for 2 hpi and two-tailed, unpaired t test for 24 hpi. (**H**) Percentage of infected or uninfected fish at 3 dpi into the HBV with 1-3 wildtype *M. marinum* with or without atorvastatin and water-soluble cholesterol. (**I**) Percentage of infected or uninfected wildtype or MYD88-depleted fish at 3 dpi into the HBV with 1-3 wildtype or Δ *mmpL7 M. marinum* with or without atorvastatin. (**H**) and (**I**) Fisher's exact test with Bonferroni's correction for multiple comparisons. (**B**)-(**D**) and (**F**)-(**I**) representative of three separate experiments.

342

343 sought to evaluate the role of statins in the reduction of bacterial burdens and in preventing

344 infection. First, we showed that statin treatment reduced bacterial burdens in the zebrafish
345 (Figure 7G). Next, to evaluate if statins prevented infection, we infected zebrafish with 1-3
346 bacteria, similar to the infectious dose in humans (Bates et al., 1965; Wells et al., 1948), and
347 evaluated their ability to establish infection. This infectivity assay previously found that PDIM-
348 deficient *M. marinum* established infection at a reduced frequency (Cambier et al., 2017). We
349 treated zebrafish with atorvastatin for 24 h prior to infection with 1-3 bacteria and continued
350 daily atorvastatin treatment for the 3-day assay period. At 3 dpi, atorvastatin treatment decreased
351 wildtype *M. marinum*'s infectivity by 50% (Figure 7H). Moreover, restoring cholesterol levels
352 by co-treating with water-soluble cholesterol restored wildtype *M. marinum*'s infectivity (Figure
353 7H). This result confirmed atorvastatin reduces infectivity by lowering cholesterol rather than to
354 its other effects on physiology and metabolism. However, this protective low-cholesterol state
355 could be due to antimicrobial effects independent of PDIM spread. Altered cholesterol flux can
356 have pleotropic effects on immunity (Tall and Yvan-Charvet, 2015), and mycobacteria have been
357 shown to use cholesterol as a carbon source (Pandey and Sassetti, 2008).
358 To test the alternative hypothesis that atorvastatin's protection is not through disrupting
359 the PDIM-TLR axis we evaluated the infectivity of PDIM-deficient Δ*mmpL7 M. marinum*.
360 Consistent with previous reports (Cambier et al., 2017), Δ*mmpL7 M. marinum* exhibited
361 decreased infectivity compared to wildtype bacteria (Figure 7I). In agreement with our model
362 that atorvastatin acts through modulating PDIM spread, we found that atorvastatin treatment did
363 not further decrease Δ*mmpL7*'s infectivity (Figure 7I). However, PDIM-deficient bacteria exhibit
364 such a severe virulence defect, any further attenuation due to other low-cholesterol-dependent
365 antimicrobial mechanisms may not be possible. To address this concern, we took advantage of
366 the fact that Δ*mmpL7*'s virulence defect is reversed in the absence of host TLR signaling (Figure
367 7I, Cambier et al., 2014b). In this condition where PDIM-deficient bacteria are fully virulent,
368 they should become attenuated by any non-PDIM-associated antimicrobial mechanisms caused
369 by atorvastatin. However, atorvastatin still did not decrease Δ*mmpL7*'s infectivity in MYD88-
370 depleted hosts (Figure 7I). Finally, we showed that atorvastatin decreased the infectivity of
371 wildtype *M. marinum* in a MYD88-dependent fashion (Figure 7I). These data strongly support
372 the idea that atorvastatin acts to disrupt the PDIM-TLR axis. Only in conditions where PDIM is
373 present on bacterial surfaces and when host TLR signaling is intact will lowering cholesterol
374 provide a protective effect. Collectively, these data demonstrate that statins reduce mycobacterial

375 infectivity by reducing host cholesterol, and thereby PDIM's infiltration of epithelial
376 membranes.
377
378 **DISCUSSION**
379 Molecular Koch's postulates are a guiding set of principles used to characterize bacterial
380 virulence factors (Falkow, 1988; 2004; Ramakrishnan, 2020). Genetic analyses are the mainstay
381 of assigning pathogenic functions to specific virulence factors, including those not directly
382 encoded by the genome. Virulence lipids are often assigned their pathogenic roles from studies
383 of bacterial mutants lacking proteins involved in the lipid's biosynthesis or transport. Thus, these
384 functions can be directly attributed only to the biosynthetic protein, and not the lipid per se.
385 Here, by combining bioorthogonal chemistry with the zebrafish model of TB, we more
386 rigorously satisfy molecular Koch's postulates to describe PDIM's role in virulence. PDIM's
387 inherent fluidity and the abundance of cholesterol in epithelial membranes influenced PDIM's
388 ability to infiltrate the host lipid environment. This occupation of epithelial membranes by PDIM
389 mediated subversion of TLR signaling at the site of infection, thus enabling mycobacteria to gain
390 access to non-activated immune cells (Figure 8).
391 The role epithelial cells play in priming innate immunity is appreciated in several models
392 of bacterial pathogenesis. *Pseudomonas aeruginosa* and *Staphylococcus aureus* are both
393 recognized by TLR-2 on human epithelial cells leading to the production of inflammatory
394 cytokines (Soong et al., 2004). In zebrafish these responses result in bacterial clearance (Cambier
395 et al., 2014b), highlighting this pathway as a conserved response to infection. In contrast, human
396 epithelial cells infected by mycobacteria have no significant change in global transcription,
397 suggesting minimal immune detection (Reuschl et al., 2017). Our data now demonstrate that
398 PDIM plays a role in silencing epithelial cell responses, promoting uptake by non-activated
399 macrophages.
400 Previous models suggest PDIM facilitates a passive evasion of TLRs by masking
401 underlying TLR ligands (Cambier et al., 2014b; 2017). This model was based on findings that
402 PDIM-expressing mycobacteria were rendered growth-attenuated if co-infected with TLR-
403 stimulating bacteria (Cambier et al., 2014b). While our current model suggests a more active role
404 for PDIM, we still find that TLR-stimulating bacteria cause attenuation of wildtype bacteria.
405 Specifically, bacteria unable to spread PDIM caused attenuation of bacteria that can spread

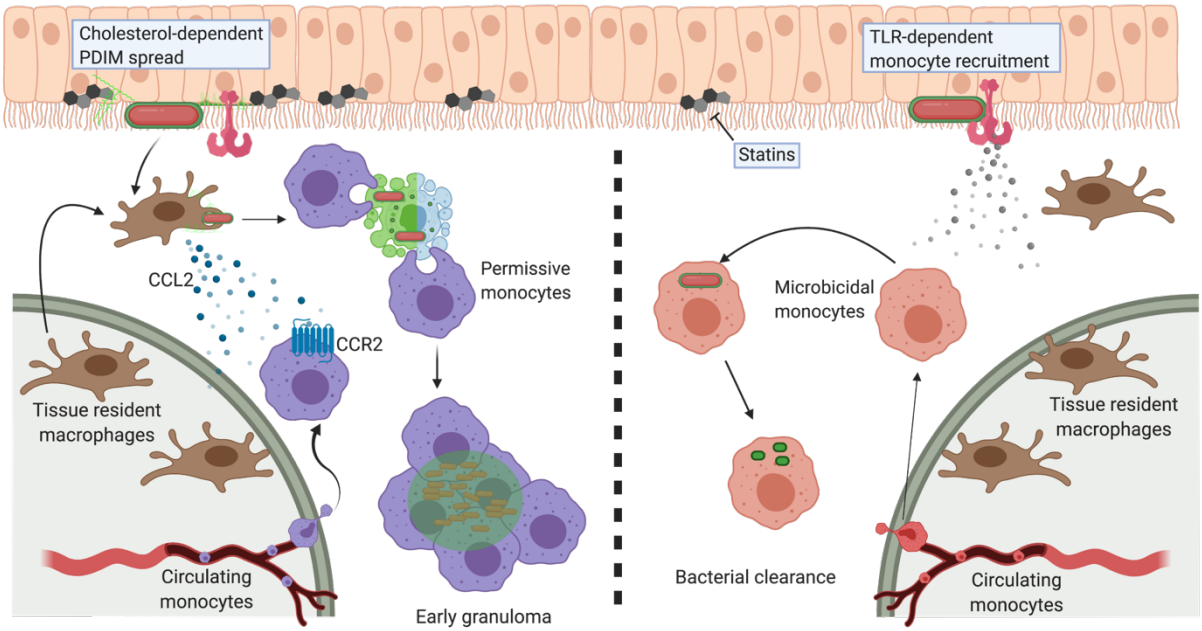

Figure 8. Model of PDIM spreading to promote virulence. Cholesterol-dependent PDIM spread into epithelial membranes prevents TLR detection at the site of infection. Bacteria then drive resident macrophages to produce CCL2 to recruit CCR2-positive permissive monocytes which go on to form early granulomas. PDIM continues to spread into host membranes throughout this process. In low cholesterol settings (statin treatment) PDIM does not spread as readily into epithelial membranes. TLR-dependent recruitment of microbicidal monocytes occurs, which can then clear infecting mycobacteria.

PDIM (Figure 6B and C). These findings argue that PDIM's influence over innate immune signaling is spatially restricted. PDIM appears to only inhibit TLR signaling at membrane sites where it has spread, emphasizing the need for PDIM localization on the bacterial surface prior to spreading into epithelial membranes. Once spread, the potential for PDIM to disrupt membrane protein signaling is intriguing. Several biophysical properties of membranes are known to mediate membrane protein function (Los and Murata, 2004), and PDIM has been implicated in altering host membrane structure (Augenstreich et al., 2019). Furthermore, TLRs have been shown to aggregate into cholesterol rich lipid domains to facilitate downstream signaling events (Ruysschaert and Lonez, 2015). How PDIM's affinity for cholesterol promotes spread and whether this association disrupts TLR-cholesterol lipid domains is yet to be determined.

The finding that PDIM's methyl-branched mycocerosic acids are required for virulence suggests pathogenic mycobacteria have evolved a lipid-based immunomodulatory strategy similar to that seen at host barrier tissues. While predominant across prokaryotes, methyl-branched fatty acids are only found in certain secretions of higher eukaryotes. In particular, vernix caseosa, a white wax that covers neonates during the third trimester of gestation, is

422 implicated in promoting normal gut development and microbial colonization (Nishijima et al.,
423 2019). The fetus swallows a significant amount of vernix shed in the amniotic fluid, in increasing
424 amounts as term birth approaches. Premature infants are exposed to substantially less vernix and
425 have increased rates of necrotizing enterocolitis (Ran-Ressler et al., 2011). In a rat model of
426 necrotizing enterocolitis, feeding premature pups methyl-branched lipids led to a decrease in
427 disease development and a shift from a pro-inflammatory to an anti-inflammatory gut
428 environment (Ran-Ressler et al., 2011). These studies implicate lipid-based immunomodulation
429 as playing a key role in tissue-barrier homeostasis, dampening immune responses to allow for
430 proper microbial colonization. Mycobacteria appear to have adapted this strategy of using
431 methyl-branched lipids as an immunomodulatory mechanism to establish infection and thereby
432 ensure their evolutionary survival.
433 Systemic cholesterol metabolism in humans influences the lung environment, including
434 the abundance of cholesterol in lung epithelial membranes (Fessler, 2017). Therefore,
435 cholesterol-promoted PDIM spreading may also influence *M. tuberculosis* transmission. While a
436 clinical trial is currently underway evaluating the use of statins alongside standard TB therapy
437 (Karakousis et al., 2019), our data instead argue for the use of statins as a TB preventative
438 therapy.
439
440 **ACKNOWLEDGEMENTS**
441 We thank Lalita Ramakrishnan for help interpreting data and manuscript writing, Karen
442 Dobos for help purifying PDIM, Benjamin M. Swarts for providing TreT-expressing *E. coli*, and
443 David Tobin for zebrafish lines. This work was supported by a National Institutes of Health grant
444 (AI51622) to C.R.B. C.J.C. was supported by a Damon Runyon Postdoctoral Fellowship. S.M.B
445 and J.A.B were supported by NIGMS F32 Postdoctoral Fellowships.
446
447 **AUTHOR CONTRIBUTIONS**
448 C.J.C., and C.R.B. conceived the project. C.J.C., S.M.B. and J.A.B. carried out
449 experiments and interpreted data. C.J.C. and C.R.B. wrote the manuscript with input from all
450 authors. C.R.B. provided supervision.
451
452

DECLARATION OF INTERESTS

C.R.B. is a co-founder of OliLux Bio, Palleon Pharmaceuticals, InverVenn Bio, Enable Biosciences, and Lycia Therapeutics, and member of the Board of Directors of Eli Lilly.

484 **MATERIALS AND METHODS**

485 **RESOURCES TABLE**

REAGENT or RESOURCE	SOURCE	IDENTIFIER
Bacterial and Virus Strains		
Mycobacterium marinum M strain transformed with pMS12:tdTomato, pMS12:EBFP2, or pMS12:wasabi	Takaki et al., 2013.	derivative of ATCC #BAA-535
Δ*mmpL7 Mycobacterium marinum* M strain transformed with pMS12:tdTomato or pMS12:wasabi	Cambier et al., 2014b.	NA
Top10 *Escherichia coli* transformed with pBAD:tret from *Thermoproteus tenax*	Urbanek et al., 2014.	NA
Chemicals, Peptides, and Recombinant Proteins		
Iodotrimethylsilane	ACROS	Cat#10530964 CAS:16029-98-4
Sodium azide	Sigma-Aldrich	Cat#S8032 CAS: 26628-22-8
Tetrabutylammonium hydroxide solution	Sigma-Aldrich	Cat#178780 CAS: 2052-49-5
Lignoceric acid	Sigma-Aldrich	Cat# L6641 CAS: 557-59-5
Click-IT Alexa Fluor 488 DIBO Alkyne	Thermo-Fisher	Cat# C10405 Discontinued*
Click-IT Alexa Fluor 647 DIBO Alkyne	Thermo-Fisher	Cat# C10408 Discontinued*
Alexa Fluor 647 Azide	Thermo-Fisher	Cat# A10277
Alkyne Cholesterol	Click Chemistry Tools	Cat# 1409
6-azido-6-deoxy-glucose	Sigma-Aldrich	Cat# 712760 CAS: 20847-05-6
UDP-glucose	Sigma-Aldrich	Cat# U4625 CAS: 28053-08-9
Alexa-647 hydroxylamine	Thermo-Fisher	Cat# A30632
Methyl-ß-cyclodextrin	Sigma-Aldrich	Cat# C4555 CAS: 128446-36-6
Cholesterol-water soluble	Sigma-Aldrich	Cat# C4951
Atorvastatin	Sigma-Aldrich	Cat# PHR1422
Methylene blue	Sigma-Aldrich	Cat# M9140 CAS: 122965-43-9
Tango Buffer (10x)	Thermo-Fisher	Cat#BY5
Phenol Red Sodium Salt	Sigma-Aldrich	Cat#P4758 CAS: 34487-61-1
PMA (Phorbol 12-myristate 13-acetate)	Sigma-Aldrich	Cat#P1585 CAS:16561-29-8
Hygromycin B	Thermo-Fisher	Cat#10687010
Glutaraldehyde solution (70% in water)	Sigma-Aldrich	Cat#G7776 CAS: 111-30-8
16% paraformaldehyde solution	Thermo-Fisher	Cat#28908
BTTP	Click Chemistry Tools	Cat#1414 CAS: 1334179-85-9
Critical Commercial Assays		

Total Cholesterol and Cholesterol Ester Colorimetric/Fluorometric Assay Kit	Bio-Vision	Cat# K603
Experimental Models: Cell Lines		
A549 human alveolar epithelial cells	ATCC	CCL-185
THP-1 human monocytic cell line	ATCC	TIB-202
Experimental Models: Organisms/Strains		
Zebrafish (Danio rerio) wild type AB strain	Stanford University	ZFIN ID: ZDB-GENO-960809-7
Zebrafish: *Tg(mfap4:tdTomato)*	Walton et al., 2015.	ZFIN ID: ZDB-TGCONSTRCT-160122-3
Oligonucleotides		
myD88 morpholino sequence: GTTAAACACTGACCCTGTGGATCAT	Bates et al., 2007.	ZFIN ID: ZDB-MRPHLNO-080325-4
Software and Algorithms		
NIS-Elements	Nikon	
Imaris	Bitplane	
Prism	GraphPad	

*Since preparing this manuscript we have found that AFDye 488 DBCO (Click Chemistry Tools, Cat# 1278) and AFDye 647 DBCO (Click Chemistry Tools, Cat# 1302) are suitable alternatives to the DIBO fluorophores. The DBCO dyes can be used with the same concentrations and labeling protocols presented in this manuscript for the DIBO dyes (Unpublished data).

Procedures and materials for synthetic chemistry: All reactions were performed in dry standard glassware fitted with rubber septa under an inert atmosphere of nitrogen unless otherwise stated. Preparative thin-layer chromatography (TLC) was performed with Millipore's 1mm and 0.2mm silica gel 60 pre-coated glass plates. Analytical TLC was used for reaction monitoring and product detection using pre-coated glass plates covered with 0.20 mm silica gel with fluorescent indicator; visualized by UV light and 10% CuSO4 in 1.3M phosphoric acid in water. Reagents were purchased in reagent grade from commercial suppliers and used as received, unless otherwise described. Anhydrous dichloromethane (DCM) was prepared by passing the solvent through an activated alumina column.

Chemical Analysis Instrumentation: Proton (^{1}H NMR) and proton-decoupled carbon-13 (^{13}C {^{1}H} NMR) nuclear magnetic resonance spectra were recorded on an Inova-500 spectrometer at 25 °C, are reported in parts per million downfield from tetramethylsilane, and are referenced to the residual protium ($CDCl_3$: 7.26 [$CHCl_3$]) and carbon ($CDCl_3$: 77.16) resonances of the NMR

505 solvent. Data are represented as follows: chemical shift, multiplicity (br = broad, s = singlet, d =
506 doublet, t = triplet, q = quartet, quin = quintet, sept = septet, m = multiplet), coupling constants in
507 Hertz (Hz), integration. Mass spectra were obtained on a Bruker Microflex MALDI-TOF by
508 mixing 0.5µl of 1mg/ml sample in chloroform with 0.5µl of 10mg/ml 2,5-dihydroxybenzoic acid
509 before spotting onto a 96-well MALDI plate.
510
511 **Isolation of PDIM**
512

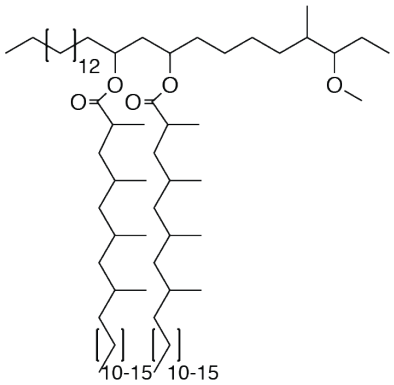

513
514
515 Wildtype *M. marinum* was grown in GAS medium without Tween-80 to an OD_{600} of 1.2.
516 Bacteria were pelleted, frozen and lyophilized on a Labconoco FreezeZone 4.5 plus. Bacterial
517 lipids were then extracted by stirring lyophilized pellet in petroleum ether for 1 h at 23 ºC.
518 Bacteria were allowed to settle, and solvent was collected. Remaining bacteria were re-extracted
519 3-5 times. The solvent extract was then passed through a 0.2µm PTFE filter, and crude lipids
520 were concentrated under reduced pressure. Crude lipid extracts were separated by preparative
521 TLC in the solvent system 98:2 petroleum ether:ethyl acetate. The band correlating to PDIM at
522 an Rf = 0.4 was isolated. Preparative TLC was repeated twice more to further purify PDIM.
523 Average PDIM isolated from *M. marinum* was 60mg per 10 liters of culture. ^{1}H NMR (500
524 MHz, $CDCl_3$) δ 4.93-4.87 (m, 2H), 3.32 (s, 3H), 2.87-2.83 (m, 1H), 2.57-2.51 (m, 2H), 1.90-0.81
525 (m, 166H). ^{13}C NMR (126 MHz, $CDCl_3$) δ 176.69, 176.63, 86.78, 86.73, 77.41, 77.37, 77.16,
526 76.90, 70.72, 70.67, 57.51, 45.56, 45.51, 41.41, 41.33, 38.56, 37.85, 37.73, 37.09, 36.77, 34.91,
527 34.18, 34.07, 32.83, 32.08, 30.24, 29.96, 29.87, 29.82, 29.75, 29.62, 29.53, 28.34, 27.64, 27.36,
528 27.25, 27.16, 27.12, 25.74, 25.35, 22.85, 22.74, 22.43, 20.81, 20.57, 20.52, 20.37, 20.27, 18.67,
529 18.58, 18.53, 14.80, 14.75, 14.28, 14.22, 10.26, 1.16. MALDI-TOF for: C82H162O5 Calc'd

530 [M+Na$^+$]=1250.23; found 1250.41. C84H166O5 Calc'd [M+Na$^+$]=1278.26, found 1278.40.
531 C86H170O5 Calc'd [M+Na$^+$]=1306.29, found 1306.55.
532
533 **Synthesis of azido-DIM**
534

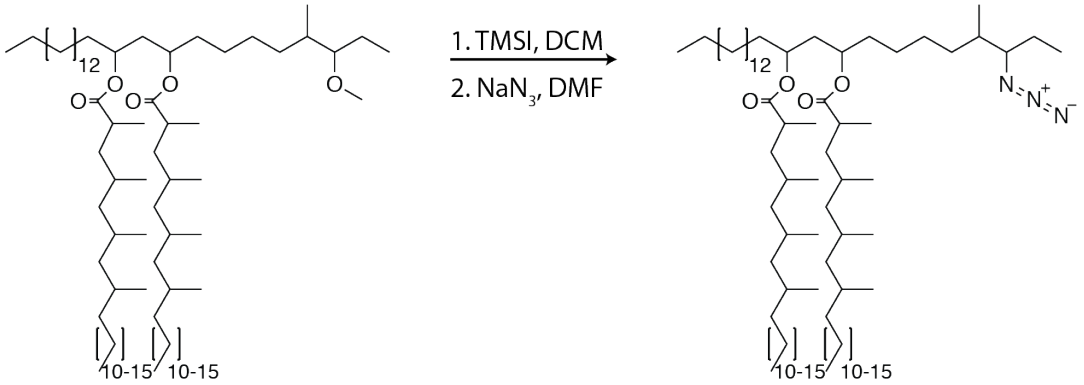

535
536
537 To PDIM (75.6mg, 60.2µmol, 1.0 equiv.) was added 0.3ml of DCM, the mixture was stirred and
538 iodotrimethylsilane (TMSI, 258µl, 1.8mmol, 30.0 equiv.) was added and allowed to react for 12
539 h at 23 ºC. The reaction was concentrated under reduced pressure. NaN3 (39.1mg, 602µmol,
540 10.0 equiv.) was added followed by 0.3ml of anhydrous dimethylformamide (DMF) and stirred
541 for 12 h at 23 ºC. The solvent was removed under reduced pressure and the product was purified
542 using preparative TLC in 98:2 petroleum ether:ethyl acetate Rf=0.5 as a white wax (37.7mg,
543 29.8µmol, 50%). ^{1}H NMR (500 MHz, $CDCl_3$) δ 5.06-4.86 (m, 2H), 3.30-3.21 (m, 1H), 2.58-2.50
544 (m, 2H) 2.1-0.81 (m, 163H). ^{13}C NMR (126 MHz, $CDCl_3$) δ 176.73, 176.63, 77.41, 77.36, 77.16,
545 76.91, 71.08, 70.74, 59.86, 45.56, 41.96, 41.45, 41.35, 39.27, 37.84, 37.73, 37.24, 37.08, 37.01,
546 35.28, 34.82, 34.18, 32.08, 30.32, 30.24, 30.22, 30.04, 29.96, 29.87, 29.82, 29.75, 29.72, 29.67,
547 29.62, 29.52, 29.39, 28.40, 28.34, 27.72, 27.36, 27.25, 27.18, 27.16, 26.20, 25.35, 25.27, 25.23,
548 22.85, 21.28, 21.13, 20.35, 20.32, 20.27, 18.73, 18.66, 18.58, 18.53, 14.56, 14.29, 13.87.
549 MALDI-TOF for: C81H159N3O4 Calc'd [M+Na$^+$]=1261.22; found 1260.92. C83H163N3O4
550 Calc'd [M+Na$^+$]=1289.25, found 1289.02. C85H167N3O4 Calc'd [M+NH4$^+$]=1312.33, found
551 1312.37.
552
553
554

555 **Hydrolysis of PDIM and isolation of phthiocerol**

556

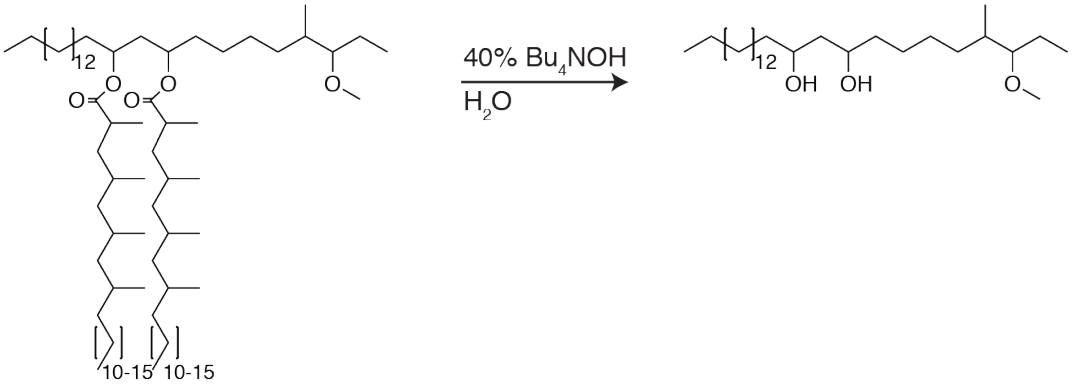

557

558

559 To dried PDIM (66.7mg, 53.1µmol) was added 0.5ml of 40% tetrabutylammonium hydroxide in
560 water, the mixture was sealed, aggressively stirred, and allowed to react for 48 h at 120 ºC.
561 Reaction was cooled to 23 ºC and 4M HCL was added dropwise until pH was < 3. The reaction
562 was extracted with DCM and washed once with water. The solvent was removed under reduced
563 pressure and phthiocerol was purified using preparative TLC in 80:20 petroleum ether:ethyl
564 acetate Rf = 0.4. (18.8mg, 42.5µmol, 80%).^{1}H NMR (500 MHz, $CDCl_3$) and ^{13}C NMR (126
565 MHz, $CDCl_3$) matched previously reported spectra. ESI HRMS for: C28H58O3 Calc'd
566 [M+H$^+$]=443.4464; found 443.4449. C29H60O3 Calc'd [M+H$^+$]=457.4621; found 457.4616.
567 C30H62O3 Calc'd [M+H$^+$]= 471.4777, found 471.4762.

568

569 **Synthesis of PDIF**

570

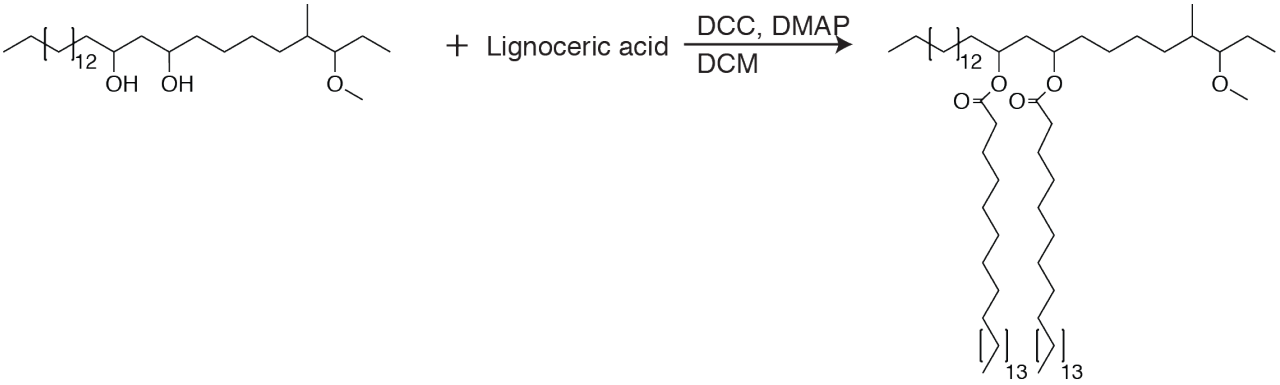

571

572

To phthiocerol (18.8mg, 42.5µmol, 1 equiv.) was added lignoceric acid (47mg, 127.5µmol, 3.0 equiv.), N,N'-dicyclohexylcarbodiimide (DCC, 35mg, 170µmol, 4.0 equiv.), 4-Dimethylaminopyridine (DMAP, 20.77mg, 170µmol, 4.0 equiv.), and 2.3ml of DCM. The reaction was stirred and allowed to react for 16 h at 23 ºC. The solvent was removed under reduced pressure and the product was purified using preparative TLC in 98:2 petroleum ether:ethyl acetate Rf=0.4. (12.8mg, 11.5µmol, 27%). ^{1}H NMR (500 MHz, $CDCl_3$) δ 4.94-4.87 (quin, 2H), 3.33 (s, 3H), 2.88-2.83 (m, 1H), 2.30-2.25 (t, 4H), 1.75-0.79 (m, 141H). ^{13}C NMR (126 MHz, $CDCl_3$) δ 173.42, 86.66, 77.27, 77.02, 76.76, 70.97, 57.40, 38.45, 34.84, 34.67, 34.13, 34.09, 32.62, 31.94, 29.73, 29.68, 29.55, 29.47, 29.38, 29.34, 29.23, 27.44, 25.57, 25.17, 25.10, 22.70, 22.37, 14.76, 14.12, 10.10. MALDI-TOF for: C76H150O5 Calc'd [M+Na$^+$]=1166.14, found 1166.14. C77H152O5 Calc'd [M+Na$^+$]=1180.15, found 1180.24. C78H154O5 Calc'd [M+Na$^+$]=1194.17; found 1194.25.

Synthesis of azido-DIF

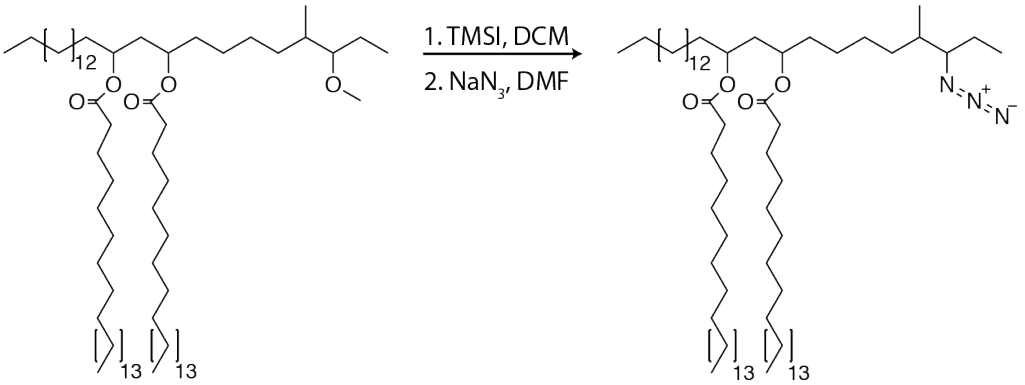

To PDIF (12.8mg, 11.5µmol, 1 equiv.) was added 0.3ml of DCM, the mixture was stirred and TMSI (49µl, 345µmol, 30.0 equiv.) was added and allowed to react for 3 h at 23 ºC. The reaction was concentrated under reduced pressure. NaN_3 (7.5mg, 115µmol, 10.0 equiv.) was added followed by 0.3ml of anhydrous dimethylformamide (DMF) and stirred for 12 h at 23 ºC. The solvent was removed under reduced pressure and the product was purified using preparative TLC in 98:2 petroleum ether:ethyl acetate Rf=0.5. (6.9mg, 6µmol, 52%). ^{1}H NMR (500 MHz, $CDCl_3$) δ 5.08-5.00 (m, 2H), 3.32-3.20 (m, 2H), 3.12-3.04 (m, 1H), 2.33-2.25 (t, 4H), 1.80-0.73 (m, 138H). ^{13}C NMR (126 MHz, $CDCl_3$) δ 173.41, 77.27, 77.02, 76.76, 71.16, 70.05, 59.72, 39.09,

598 36.92, 35.12, 34.70, 34.64, 32.34, 31.94, 29.72, 29.67, 29.58, 29.53, 29.42, 29.38, 29.33, 29.23,
599 26.05, 25.15, 24.02, 22.70, 21.15, 16.10, 14.13, 11.06, 1.03. ESI C75H148NO4 calc'd [M+K, -
600 N_2]=1166.10, found 1166.05.
601
602 **Zebrafish Husbandry and Infections**
603 Wild-type AB (Zebrafish International Resource Center), and *Tg(mfap4:tdTomato)* (Walton et
604 al., 2015) lines were maintained in buffered reverse osmotic water systems. Fish were fed twice
605 daily a combination of dry feed and brine shrimp and were exposed to a 14 h light, 10 h dark
606 cycle to maintain proper circadian conditions. Zebrafish embryos were maintained at 28.5 ºC in
607 embryo media which consisted of the following dissolved in Milli-Q water (%weight/volume): 0.
608 0875% sodium chloride, 0.00375% potassium chloride, 0.011% calcium chloride, 0.00205%
609 monopotassium phosphate, 0.00089% disodium phosphate, and 0.0493% magnesium sulfate.
610 Embryo media was then buffered to pH 7.2 with sodium bicarbonate. Embryos were maintained
611 in 0.25 mg/ml methylene blue (Sigma) from collection to 1-day post-fertilization (dpf). 0.003%
612 PTU (1-phenyl-2-thiourea, Sigma) was added from 24 h post-fertilization (hpf) on to prevent
613 pigmentation. Larvae (of undetermined sex given the early developmental stages used) were
614 infected at 48 hpf via the hindbrain ventricle (HBV) using single-cell mycobacterial suspensions
615 of known titer. Number of animals to be used for each experiment was guided by pilot
616 experiments or by past results with other bacterial mutants and/or zebrafish. On average 15 to 40
617 larvae per experimental condition were required to reach statistical significance and each
618 experiment was repeated at least three times. Larvae were randomly allotted to the different
619 experimental conditions. The zebrafish husbandry briefly described above and all experiments
620 performed on them were in compliance with the U.S. National Institutes of Health guidelines and
621 approved by the Stanford Institutional Animal Care and Use Committee.
622
623 **Bacterial Strains and Methods**
624 *M. marinum* strain M (ATCC BAA-535) and Δ*mmpL7* mutants (Cambier et al., 2014b)
625 expressing either TdTomato, Wasabi, or EBFP2 under the control of the *msp12* promoter were
626 grown under hygromycin (Thermo-Fisher) selection in 7H9 Middlebrook's medium (Difco)
627 supplemented with 10% OADC (Fisher), 0.2% glycerol, and 0.05% Tween-80 (Sigma). Where
628 noted bacteria were also grown in glycerol-alanine-salts (GAS) medium, recipe

629 (%weight/volume) in 18mM sodium hydroxide in Milli-Q water pH 6.6 +/- 0.05% Tween-80:
630 0.03% BactoCasitone (BD Science), 0.005% ferric ammonium citrate (Sigma), 0.4% potassium
631 phosphate dibasic anhydrous (VWR), 0.2% citric acid, anhydrous (VWR), 0.1% L-alanine
632 (Sigma), 0.12% magnesium chloride, heptahydrate (VWR), 0.06% potassium sulfate (VWR),
633 0.2% ammonium chloride (VWR), and 1% glycerol. To prepare heat-killed *M. marinum*, bacteria
634 were incubated at 80ºC for 20 min. To prepare fixed bacteria, bacteria were incubated in
635 described concentrations of glutaraldehyde (Sigma) and/or paraformaldehyde (Thermo-Fisher)
636 for 1hr at 23ºC, followed by 3 washes with PBS prior to experimental use.
637
638 **Cell Lines and infections**
639 Cells were grown in T75 flasks (Thermo-Fisher) and maintained at 37 °C and 5% CO2. THP-1
640 were grown in RPMI supplemented with 10% fetal bovine serum (FBS). A549 were grown in
641 DMEM supplemented with 10% FBS. Two days prior to infection, THP-1s were plated on 8-
642 well Nunc Lab-Tek II chamber slides (Thermo-Fisher) at a density of 150,000 cells per well with
643 100nM PMA (phorbol 12-myristate 13-acetate, Sigma) in growth media and incubated at 37ºC
644 and 5% CO2 for 24 h. One day prior to infection, the media on THP-1s was replaced with fresh
645 growth media and the cells were incubated at 33ºC and 5% CO2 for 24 h, cells were then
646 infected with *M. marinum* at a multiplicity of infection (MOI) of 2 in growth media. Infection
647 was allowed to progress for 6 h prior to washing twice with PBS and replacing with growth
648 media. THP-1s were then incubated for 24 h at 33ºC and 5% CO2 prior to experimental end
649 point. One day prior to infection, A549s were plated on 8-well chamber Nunc Lab-Tek II
650 chamber slides (Thermo-Fisher) at a density of 50,000 cells per well in growth media and
651 incubated at 37ºC and 5% CO2. Day of infection cells were moved to 33ºC and 5% CO2 for 3 h,
652 and then were infected with *M. marinum* at a MOI of 5 and incubated at 33ºC and 5% CO2 for
653 24 h. Infected THP-1s and A549s were then imaged as described below.
654
655 **Extraction and reconstitution of *M. marinum***
656 *Extraction*. 1 liter of *M. marinum* were grown in GAS medium plus Tween-80 to an OD_{600} of
657 1.2. Bacteria were pelleted in a glass 50mL conical tubes (Fisher) of known weight, frozen and
658 lyophilized. The dry bacteria in 50mL conical tubes were then weighed and the dry bacterial
659 weight was calculated. 25mL of petroleum ether were then added to the bacteria, and the conical

660 tube was capped with a PTFE lined lid (Sigma) and the suspension was vortexed for 3min. An
661 additional 25mL of petroleum ether was added and the sample was centrifuged for 3min at
662 1000xg at 4ºC. The extract was then saved or discarded depending on the downstream
663 experimental applications and the bacteria were extracted once more as above. For total lipid
664 extractions (not used for reconstitution), bacteria were treated with 1:1 chloroform:methanol for
665 12 h at 60ºC. Extracts were filtered, back extracted with water to remove water soluble
666 contaminants, dried under reduced pressure and used for downstream experiments.
667
668 *Reconstitution.* Prior to extractions the following calculation was used to determine the amount
669 of lipids to add back to each pellet.
670
671 (23mg lipid/gram dry bacteria)*(weight in grams of dry bacteria)/(0.75 reconstitution efficiency)
672
673 Where 23mg of lipid per gram of dry bacteria is the experimentally determined average amount
674 of lipid removed during petroleum ether extraction of bacteria grown in these conditions (Figure
675 S1B, initial extraction) and the 0.75 reconstitution efficiency was also experimentally determined
676 (Figure S1C). If reconstituting with DIM variants, 30% of the above weight consists of DIMs
677 and the remainder will consist of DIM-depleted petroleum ether lipid extracts. Following two
678 rounds of petroleum ether extraction as detailed above, bacteria were immediately mixed with
679 pre-determined lipid mixtures (or no lipid at all for delipidated bacteria) in petroleum ether (2-3
680 mls) followed by extended drying under reduced pressure. Dried bacteria were then rescued into
681 7H9 media supplemented with 10% OADC, and 0.2% glycerol (prep media) and subjected to
682 single cell preparation protocol.
683
684 ***M. marinum* single cell preparation**
685 For more thorough details, as well as rationale and explanation of the following protocol see
686 Takaki et al., 2013. Bacteria were washed once with 15mL of prep media followed by
687 resuspension in 500µl of prep media. Bacteria were then passed through a 27-gauge needle 10
688 times, followed by the addition of 1ml of prep media and centrifugation at 100xg for 3min. 1ml
689 of supernatants were saved. This process was repeated 3-5 times. Collected supernatants were
690 then passed through a 5.0µm acrodisc versapor membrane syringe filter (VWR). The filtrate was

691 then pelleted at 16,000xg for 2min, pellets were resuspended in prep media to a concentration of
692 around 1x10^8-9 bacteria per ml, aliquoted and stored at -20C for future use, or immediately
693 subjected to copper-free click chemistry reactions.
694
695 **Metabolic labeling of *M. marinum* with 6-TreAz**
696 *Expression and Purification of TreT*: TreT was expressed and purified utilizing a similar method
697 as previously reported (Urbanek et al., 2014). Top10 *E. coli* expressing the *tret* gene from
698 *Thermoproteus tenax* (pBAD plasmid, AraC control) were streaked onto a Lysogeny broth (LB)
699 agar plate supplemented with 100 µg/mL ampicillin and incubated at 37 °C for 24 h. A single
700 colony was picked and used to inoculate 5 mL of LB liquid medium containing 100 µg/mL
701 ampicillin. The starter culture was placed in a shaking incubator (175 rpm) at 37 °C for 16 h. The
702 starter culture was then transferred to a 1 L solution of sterilized Terrific broth (TB)
703 supplemented with 100 µg/mL ampicillin in a sterilized 2 L Fernbach culture flask. The flask
704 was shaken (175 rpm) at 37 °C. When the absorbance at 600 nm reached between 0.6 and 0.9
705 (typically 4-5 h post inoculation), TreT expression was induced by adding 1 mL of 1 M
706 arabinose solution in sterile water (1 mM final concentration). The flask was again shaken (175
707 rpm) at 37 °C for another 20 h. The culture was then transferred to a polypropylene bottle and
708 pelleted for 15 minutes at 4,000 x g at 4 °C. The supernatant was discarded, and the pellet was
709 suspended in 45 mL of lysis buffer (50 mM NaH_2PO_4, 500 mM NaCl, 20 mM imidazole, pH 7.4)
710 and run through a homogenizer 5 times utilizing ice to keep the solution cool. Once
711 homogenized, the lysate was clarified by centrifugation pelleting for 20 minutes at 21,000 x g at
712 4 °C and filtering through a 0.45 µm Teflon syringe filter. To the clarified lysate (generally about
713 50 mg/mL protein content as measured with absorbance at 280 nm) was then added 5 mL of pre-
714 washed (lysis buffer) Ni-NTA resin slurry (Qiagen). The suspension was mixed on an orbital
715 shaker for 60 – 90 minutes at 4 °C and then transferred to a glass column (BIO-RAD
716 EconoColumn). Non-His-Tagged proteins were eluted with lysis buffer until the absorbance at
717 280 nm matched background levels utilizing 50 – 100 mL of lysis buffer. His-tagged TreT was
718 eluted with elution buffer (50 mM NaH_2PO_4, 500 mM NaCl, 250 mM imidazole, pH 7.4) in
719 multiple 2.5 mL increments, until protein elution was determined complete by absorbance at 280
720 nm. Buffer exchange to a storage/reaction buffer (50 mM Tris, 300 mM NaCl, pH 8.0) was
721 performed with a desalting column (PD-10, GE Healthcare) and the protein was transferred to a

722 conical tube and diluted to 1 mg/mL as determined by absorbance at 280 nm for long-term
723 storage. Storage of the enzyme at 4 °C and at this concentration yields active protein that does
724 not have significant losses in activity even after 12 months of storage under these conditions.
725
726 *Synthesis and Purification of 6-Azido-6-deoxy-trehalose (6-TreAz):* To a 1.5 mL Eppendorf tube
727 was added 200 µL of a 100 mM solution of 6-azido-6-deoxy-glucose (final concertation 20 mM),
728 100 µL of a freshly-prepared 400 mM solution of UDP-glucose (final concentration 40 mM),
729 100 µL of a 200 mM solution of $MgCl_2$ (final concentration 20 mM), and 300 mL of reaction
730 buffer (50 mM Tris, 300 mM NaCl, pH 7.4). Then, 300 µL of TreT solution in storage/reaction
731 buffer was added (final concentration 300 µg/mL) and the reaction vessel was closed and mixed
732 gently by inverting the tube. The reaction was heated to 70 °C for 60 – 90 minutes with shaking
733 at 400 rpm and then cooled on ice before further manipulation. The reaction contents were
734 transferred to a pre-washed Amicon centrifugal filter with a nominal molecular weight limit
735 (NWML) of 10 kDa. The filter was washed with DI water (2 x 1 mL) to facilitate maximal
736 recovery. The upper chamber was discarded and 1 g of prewashed mixed-bed ion-exchange resin
737 (DOWEX) was added to the filtrate and the slurry was equilibrated for 60 – 90 minutes. The
738 suspension was filtered, and the resin was rinsed with 3 – 5 mL of DI water. Analysis by TLC
739 (5:3:2 *n*-butanol: ethanol: DI water) and/or LC-MS equipped with a Supelco aminopropyl
740 column [4.6 x 250 mm, 5 µm] (isocratic 80% ACN in DI water, 0.5 mL/min flowrate) indicated
741 full and complete conversion of 6-azido-6-deoxy-glucose to 6-azido-6-deoxy-trehalose with high
742 purity as determined by nuclear magnetic resonance (NMR), which matched previously reported
743 spectra.
744
745 *Synthesis and Direct utilization of 6-TreAz for labeling Mycobacterium marinum*: To facilitate
746 easier production and labeling of *M. marinum* with 6-TreAz, the reaction was performed as
747 above but 6-TreAz was not isolated prior to labeling. Upon reaction completion, the reaction was
748 cooled on ice to bring the vessel back to ambient temperature. The 10 mM stock of 6-TreAz was
749 then added to cultures of *Mycobacterium marinum* to a final concentration of 50 µM.
750
751
752

753 **Periodate-hydroxylamine staining of mycobacterial surfaces**

754 Surface-exposed terminal oxidizable carbohydrates were labeled with hydroxylamine following
755 periodate oxidation. Lyophilized control or reconstituted *M. marinum* were washed twice with
756 PBS and resuspended in 0.1 M sodium acetate (Sigma), pH 5.5 containing 1 mM sodium
757 periodate (Sigma). Following a 20-min incubation at 4°C with gentle rotation, 0.1 mM glycerol
758 was added to stop the reaction. Cultures were washed three times with PBS and then subjected to
759 single cell preparation. Following single cell preparation, pellets were transferred to a 96-well
760 plate and then incubated with PBS containing 1 mM Alexa-647 hydroxylamine (Thermo-Fisher).
761 Following a 2 h incubation at 23 ºC, the cultures were washed 5 times with PBS and twice with
762 prep media.

763

764 **Copper-free click chemistry of *M. marinum***

765 Following reconstitution or metabolic labeling, bacteria were treated for single cell preparation.
766 Bacteria were then transferred to 96-well v-bottom dishes and were washed twice with PBS
767 using centrifugation at 3000xg for 3min between washing. Bacteria were then stained with either
768 5µM DIBO-488 (Thermo-Fisher), or 30µM DIBO-647 (Thermo-Fisher) in 200µl PBS for 90min
769 at 23 ºC protected from light. Bacteria were then washed 5 times in PBS followed by 2 washes in
770 prep media. Bacteria were then aliquoted and stored at -20C for future use. Staining efficiency
771 was evaluated by flow cytometry on a BD-Accuri C6 Plus and analysis was performed using the
772 FlowJo software package. Staining was also evaluated by microscopy with a 60x oil-immersion
773 Plan Apo 1.4 NA objective on the Nikon A1R confocal microscope.

774

775 **MYD88 morpholino and liposome injections**

776 To generate MYD88 knockdown zebrafish larvae, the MYD88 morpholino
777 5'GTTAAACACTGACCCTGTGGATCAT3' (Bates et al., 2007) was diluted to 2mM in 0.5 x
778 tango buffer (Thermo Scientific), containing 2% phenol red sodium salt solution (Sigma). 1 nl of
779 the morpholino mixture was injected into the 1-4 cell stage of the developing embryo. Lipo-PBS
780 and lipo-clodronate (http://clodronateliposomes.org) were diluted 1:10 in PBS and injected into
781 2-dpf-old larvae in ~10 nl via the caudal vein.

782

783

784 **Confocal microscopy and image-based quantification of infection**
785 Larvae were embedded in 1.5% low melting point agarose (Thermo-Fisher) and a series of z
786 stack images with a 2µm step size was generated through the infected HBV. For infected THP-1
787 and A549 cells, a series of z stack images with a 1µm step size was generated. Images were
788 captured using the galvo scanner (laser scanner) of the Nikon A1R confocal microscope with a
789 20x Plan Apo 0.75 NA objective. Higher resolution images were generated using a 40x water-
790 immersion Apo 1.15 NA objective. Bacterial burdens were determined by using the 3D surface-
791 rendering feature of Imaris (Bitplane Scientific Software). Spread lipid images were generated
792 by subtracting the bacterial surface from the lipid channel. 3D surface-rendering was then done
793 in Imaris on both the total lipid and spread lipid images to generate a percent spread value.
794
795 **Macrophage and Monocyte hindbrain recruitment assay**
796 For the macrophage recruitment (Figure 1G): 2 dpf zebrafish were infected in the HBV with *M.*
797 *marinum* at the dose reported in the figure legends. At 3 h post infection, the number of total
798 myeloid cells in the HBV was quantified using differential interference contrast microscopy
799 using a 20x Plan Fluor 0.75 NA objective on Nikon's Ti eclipse inverted microscope. For
800 quantification of monocytes (Figure 5A and B): 2 dpf zebrafish were injected in the caudal vein
801 with 200µg/ml of the nuclear stain Hoechst 33342 (Thermo-Fisher) 2 hours prior to HBV
802 infection. Hoechst is unable to cross the blood-brain barrier and therefore will label circulating
803 monocytes but will not label brain resident macrophages (Cambier et al., 2017). At 3hpi blue-
804 fluorescent cells in the hindbrain was quantified similar to above macrophage recruitment assay.
805
806 **Co-infection Experiments**
807 Around 40-50 tdTomato expressing wildtype *M. mairnum* were co-infected with an equal
808 number of wasabi expressing *M. marinum* into the HBV. At 3 dpi the bacterial volume of the
809 wildtype tdTomato expressing *M. marinum* was quantified as described above (*Confocal*
810 *microscopy and image-based quantification of infection*).
811
812 **Infectivity Assay**
813 3 days post fertilization larvae were infected via the hindbrain ventricle with an average of 0.8
814 bacteria per injection. Fish harboring 1-3 bacteria were identified at 5 h post infection by

815 confocal microscopy. These infected fish were then evaluated at 3 dpi and were scored as
816 infected or uninfected, based on the presence or absence of fluorescent bacteria.
817
818 **Fluorescence recovery after photobleaching (FRAP) experiments**
819 FRAP experiments were performed using the galvo scanner (laser scanner) of the Nikon A1R
820 confocal microscope with a 60x oil-immersion Plan Apo 1.4 NA objective. Photobleaching was
821 performed with the 405 nm laser for 200ms on a region of interest (ROI) encompassing ~1µm
822 from one pole of a single bacteria. A series of images was taken every second over the course of
823 31 seconds, one prior to bleaching. Labeled cells were mounted on a slide and coverslip in
824 0.75% low melting agarose. NIS Elements software (Nikon) was used to analyze the FRAP data
825 to extract the fluorescence recovery kinetics. Briefly, the first image before photobleaching was
826 used to generate an ROI for the entire cell and a second ROI was generated in the photobleached
827 area. Total fluorescence intensities in both the whole cell area and the bleached area were
828 extracted and normalized to correct for photobleaching of the dyes due to acquisition. The
829 normalized fluorescence intensities of the bleached area were then fitted to a non-linear
830 regression with a one-phase association, with the plateau values from each sample plotted to
831 represent the mobile fraction.
832
833 **Alkyne-cholesterol labeling of *M. marinum***
834 Wildtype or Δ*mmpL7 M. marinum* expressing wasabi fluorescent protein were grown in 7H9
835 medium supplemented with 10% OADC, 0.2% glycerol with or without 0.005% alkyne-
836 cholesterol for 48 h. Bacteria were then washed 3x with PBS prior to the copper-click reaction
837 with AlexaFluor-647 Azide. For copper click: 400µM BTTP (Click Chemistry Tools) and
838 200µM copper sulfate (Sigma) were dissolved in PBS and allowed to complex for 20 minutes.
839 30µM AlexaFluor-647 Azide (Thermo-Fisher) and 1.2mM sodium ascorbate (Sigma) were then
840 added to the solution. Bacterial pellets in 96-well v-bottom plates were resuspended in 50µl of
841 the solution and were incubated at 23 ºC protected from light for 45 minutes. Bacteria were then
842 washed 5x in PBS prior to imaging on a Nikon A1R confocal microscope with a 60x oil-
843 immersion Plan Apo 1.4 NA objective. Nikon elements software was used to determine
844 fluorescent intensities of wasabi and cholesterol signals calculated from line profiles drawn
845 perpendicular to bacterial membranes at least 0.5µm from either pole.

846

847 **Cholesterol depletion and infection of A549 epithelial cells**

848 A549 cells were seeded at 50,000 cells per 8-well Nunc Lab-Tek II chambered coverglass or at
849 100,000 cells per well in a 24 well plate. Cells were incubated at 37 ºC for 48 h. Cells were
850 washed 1x in PBS followed by treatment with 10mM methyl-ß cyclodextrin (Sigma), 1mM
851 water-soluble cholesterol (Sigma), or a combination of 10mM methyl-ß cyclodextrin and 1mM
852 water-soluble cholesterol in serum free DMEM media. Cells were treated for 1 hour at 33 ºC
853 followed by 3 washes with PBS. Cells plated on chambered coverglass were infected with azido-
854 DIM labeled *M. marinum* at an MOI of 5 for 24 h at 33 ºC followed by imaging on a Nikon A1R
855 confocal microscope with a 20x Plan Apo 0.75 NA objective. 2µm z-stacks were generated
856 through the infected cells. Azido-DIM spreading was calculated similar to above (Section:
857 *Confocal microscopy and image-based quantification of infection*). Cells plated on 24-well plates
858 were rescued in DMEM + 10% FBS for 3 h at 33 ºC. Cells were then harvested for
859 quantification of cholesterol levels.

860

861 **Atorvastatin treatment of zebrafish larvae**

862 At 48 h post fertilization, 0.5µM atorvastatin (Sigma), or 10µM water-soluble cholesterol
863 (Sigma), or both were added to zebrafish water containing 1% DMSO. Control fish were
864 incubated in water with 1% DMSO only. Zebrafish were incubated for 24 h prior to infection or
865 to cholesterol quantification. Drugs were replenished every 24 h until experiment endpoint.

866

867 **Quantification of cholesterol in zebrafish and A549 epithelial cells**

868 Cholesterol was quantified using the Total Cholesterol and Cholesterol Ester
869 Colorimetric/Fluorometric Assay Kit (BioVision). For zebrafish, 8 larvae were euthanized,
870 transferred to a 1.5ml Eppendorf tube and excess water was removed. A solution of
871 chloroform:isopropanol:NP-40 (7:11:0.1) was added and the sample was sonicated in a water
872 bath for 1 hour. Samples were then centrifuged at 16,000xg for 10min and supernatants were
873 transferred to a fresh tube and were allowed to dry in a 60 ºC water in a chemical fume hood. For
874 A549 epithelial cells, chloroform:isopropanol:NP-40 (7:11:0.1) was added directly to cells in a
875 24 well plate. Cells were scrapped and solution was transferred to a 1.5ml Eppendorf tube and
876 was centrifuged at 16,000xg for 10min and supernatants were transferred to a fresh tube and

877 were allowed to dry in a 60 ºC water in a chemical fume hood. Dried lipids were then subjected
878 to manufacturer's protocol and total cholesterol concentrations were determined by fluorescence
879 on a SpectraMax i3x plate reader (Molecular Devices).
880
881 **Statistics**
882 Statistical analyses were performed using Prism 8.4.3 (GraphPad): When appropriate
883 D'Agostino-Pearson normality test was done to determine if all of the groups in a particular data
884 set were of a gaussian distribution which then guided the subsequent statistical test performed
885 (Supplemental Table 1). Where the *n* value is given and not represented graphically in the figure,
886 *n* represents the number of zebrafish used for each experimental group (Figure 7H and I).
887
888 **REFERENCES**

889 Anderson, R.J. (1929). The chemistry of the lipoids of tubercle bacilli iv. concerning the so
890 called tubercle bacilli wax. analysis of the purified wax. J. Biol. Chem. *83*, 505–522.

891 Astarie-Dequeker, C., Le Guyader, L., Malaga, W., Seaphanh, F.-K., Chalut, C., Lopez, A., and
892 Guilhot, C. (2009). Phthiocerol Dimycocerosates of M. tuberculosis Participate in Macrophage
893 Invasion by Inducing Changes in the Organization of Plasma Membrane Lipids. PLoS Pathog *5*,
894 e1000289–16.

895 Augenstreich, J., Arbues, A., Siméone, R., Haanappel, E., Wegener, A., Sayes, F., Le Chevalier,
896 F., Chalut, C., Malaga, W., Guilhot, C., et al. (2017). ESX-1 and phthiocerol dimycocerosates of
897 Mycobacterium tuberculosis act in concert to cause phagosomal rupture and host cell apoptosis.
898 Cellular Microbiology *19*.

899 Augenstreich, J., Haanappel, E., Ferré, G., Czaplicki, G., Jolibois, F., Destainville, N., Guilhot,
900 C., Milon, A., Astarie-Dequeker, C., and Chavent, M. (2019). The conical shape of DIM lipids
901 promotes Mycobacterium tuberculosis infection of macrophages. Proceedings of the National
902 Academy of Sciences *3*, 201910368.

903 Barczak, A.K., Avraham, R., Singh, S., Luo, S.S., Zhang, W.R., Bray, M.-A., Hinman, A.E.,
904 Thompson, M., Nietupski, R.M., Golas, A., et al. (2017). Systematic, multiparametric analysis of
905 Mycobacterium tuberculosis intracellular infection offers insight into coordinated virulence.
906 PLoS Pathog *13*, e1006363–27.

907 Bates, J.H., Potts, W.E., and Lewis, M. (1965). Epidemiology of Primary Tuberculosis in an
908 Industrial School. N. Engl. J. Med. *272*, 714–717.

909 Bates, J.M., Akerlund, J., Mittge, E., and Guillemin, K. (2007). Intestinal alkaline phosphatase
910 detoxifies lipopolysaccharide and prevents inflammation in zebrafish in response to the gut
911 microbiota. Cell Host & Microbe *2*, 371–382.

912 Beatty, W.L., Rhoades, E.R., Ullrich, H.J., Chatterjee, D., Heuser, J.E., and Russell, D.G. (2000).
913 Trafficking and release of mycobacterial lipids from infected macrophages. Traffic *1*, 235–247.

914 Bernut, A., Herrmann, J.-L., Kissa, K., Dubremetz, J.-F., Gaillard, J.-L., Lutfalla, G., and
915 Kremer, L. (2014). Mycobacterium abscessus cording prevents phagocytosis and promotes
916 abscess formation. Proceedings of the National Academy of Sciences *111*, E943–E952.

917 Brzostek, A., Pawelczyk, J., Rumijowska-Galewicz, A., Dziadek, B., and Dziadek, J. (2009).
918 Mycobacterium tuberculosis Is Able To Accumulate and Utilize Cholesterol. Journal of
919 Bacteriology *191*, 6584–6591.

920 Budin, I., de Rond, T., Chen, Y., Chan, L.J.G., Petzold, C.J., and Keasling, J.D. (2018). Viscous
921 control of cellular respiration by membrane lipid composition. Science *362*, 1186–1189.

922 Camacho, L.R., Constant, P., Raynaud, C., Lanéelle, M.-A., Triccas, J.A., Gicquel, B., Daffé,
923 M., and Guilhot, C. (2001). Analysis of the Phthiocerol Dimycocerosate Locus of
924 Mycobacterium tuberculosis. J. Biol. Chem. *276*, 19845–19854.

925 Cambier, C.J., Falkow, S., and Ramakrishnan, L. (2014a). Host evasion and exploitation
926 schemes of Mycobacterium tuberculosis. Cell *159*, 1497–1509.

927 Cambier, C.J., O'Leary, S.M., O'Sullivan, M.P., Keane, J., and Ramakrishnan, L. (2017).
928 Phenolic Glycolipid Facilitates Mycobacterial Escape from Microbicidal Tissue-Resident
929 Macrophages. Immunity *47*, 552–565.e554.

930 Cambier, C.J., Takaki, K.K., Larson, R.P., Hernandez, R.E., Tobin, D.M., Urdahl, K.B., Cosma,
931 C.L., and Ramakrishnan, L. (2014b). Mycobacteria manipulate macrophage recruitment through
932 coordinated use of membrane lipids. Nature *505*, 218–222.

933 Cohen, S.B., Gern, B.H., Delahaye, J.L., Adams, K.N., Plumlee, C.R., Winkler, J.K., Sherman,
934 D.R., Gerner, M.Y., and Urdahl, K.B. (2018). Alveolar Macrophages Provide an Early
935 Mycobacterium tuberculosis Niche and Initiate Dissemination. Cell Host & Microbe *24*, 439–
936 446.e4.

937 Comas, I., Coscolla, M., Luo, T., Borrell, S., Holt, K.E., Kato-Maeda, M., Parkhill, J., Malla, B.,
938 Berg, S., Thwaites, G., et al. (2013). Out-of-Africa migration and Neolithic coexpansion of
939 Mycobacterium tuberculosis with modern humans. Nat. Genet. *45*, 1176–1182.

940 Cox, J.S., Chen, B., McNeil, M., and Jacobs, W.R. (1999). Complex lipid determines tissue-
941 specific replication of Mycobacterium tuberculosis in mice. Nature *402*, 79–83.

942 Davis, J.M., and Ramakrishnan, L. (2009). The role of the granuloma in expansion and
943 dissemination of early tuberculous infection. Cell *136*, 37–49.

944 Dutta, N.K., Bruiners, N., Pinn, M.L., Zimmerman, M.D., Prideaux, B., Dartois, V., Gennaro,
945 M.L., and Karakousis, P.C. (2016). Statin adjunctive therapy shortens the duration of TB
946 treatment in mice. J. Antimicrob. Chemother. *71*, 1570–1577.

947 Falkow, S. (1988). Molecular Koch's postulates applied to microbial pathogenicity. Rev. Infect.
948 Dis. *10 Suppl 2*, S274–S276.

949 Falkow, S. (2004). Molecular Koch's postulates applied to bacterial pathogenicity--a personal
950 recollection 15 years later. Nat. Rev. Microbiol. *2*, 67–72.

951 Fessler, M.B. (2017). A New Frontier in Immunometabolism. Cholesterol in Lung Health and
952 Disease. Ann Am Thorac Soc *14*, S399–S405.

953 Gatfield, J., and Pieters, J. (2000). Essential role for cholesterol in entry of mycobacteria into
954 macrophages. Science *288*, 1647–1650.

955 Howell, J.I., Ahkong, Q.F., Cramp, F.C., Fisher, D., Tampion, W., and Lucy, J.A. (1972).
956 Membrane fluidity and membrane fusion. Biochem. J. *130*, 44P–44P.

957 Huebinger, J., Spindler, J., Holl, K.J., and Koos, B.X.R. (2018). Quantification of protein
958 mobility and associated reshuffling of cytoplasm during chemical fixation. Scientific Reports 1–
959 11.

960 Indrigo, J. (2003). Cord factor trehalose 6,6'-dimycolate (TDM) mediates trafficking events
961 during mycobacterial infection of murine macrophages. Microbiology *149*, 2049–2059.

962 Jackson, M. (2014). The mycobacterial cell envelope-lipids. Cold Spring Harb Perspect Med *4*.

963 Jung, M.E., and Lyster, M.A. (1977). Quantitative dealkylation of alkyl ethers via treatment with
964 trimethylsilyl iodide. A new method for ether hydrolysis. J. Org. Chem. *42*, 3761–3764.

965 Kamariza, M., Shieh, P., Ealand, C.S., Peters, J.S., Chu, B., Rodriguez-Rivera, F.P., Babu Sait,
966 M.R., Treuren, W.V., Martinson, N., Kalscheuer, R., et al. (2018). Rapid detection of
967 Mycobacterium tuberculosis in sputum with a solvatochromic trehalose probe. Sci Transl Med
968 *10*, eaam6310.

969 Karakousis, P.C., Chaisson, R.E., Martinson, N. (2019) StAT-TB (Statin Adjunctive Therapy for
970 TB): A Phase 2b Dose-finding Study of Pravastatin in Adults with Tuberculosis. National
971 Institute of Allergy and Infectious Diseases. https://clinicaltrials.gov/ct2/show/NCT03882177

972 Kim, M.-C., Yun, S.-C., Lee, S.-O., Choi, S.-H., Kim, Y.S., Woo, J.H., and Kim, S.-H. (2019).
973 Association between Tuberculosis, Statin Use, and Diabetes: A Propensity Score–Matched
974 Analysis. The American Journal of Tropical Medicine and Hygiene *101*, 350–356.

975 Kondo, E., and Kanai, K. (1976). A suggested role of a host-parasite lipid complex in
976 mycobacterial infection. Jpn. J. Med. Sci. Biol. *29*, 199–210.

977 Lai, C.-C., Lee, M.-T.G., Lee, S.-H., Hsu, W.-T., Chang, S.-S., Chen, S.-C., and Lee, C.-C.
978 (2016a). Statin treatment is associated with a decreased risk of active tuberculosis: an analysis of
979 a nationally representative cohort. Thorax *71*, 646–651.

980 Lai, C.-C., Lee, M.-T.G., Lee, S.-H., Hsu, W.-T., Chang, S.-S., Chen, S.-C., and Lee, C.-C.
981 (2016b). Statin treatment is associated with a decreased risk of active tuberculosis: an analysis of
982 a nationally representative cohort. Thorax *71*, 646–651.

983 Lerner, T.R., Queval, C.J., Fearns, A., Repnik, U., Griffiths, G., and Gutierrez, M.G. (2017).
984 Phthiocerol dimycocerosates promote access to the cytosol and intracellular burden of
985 Mycobacterium tuberculosis in lymphatic endothelial cells. 1–13.

986 Los, D.A., and Murata, N. (2004). Membrane fluidity and its roles in the perception of
987 environmental signals. Biochimica Et Biophysica Acta (BBA) - Biomembranes *1666*, 142–157.

988 Maerz, L.D., Burkhalter, M.D., Schilpp, C., Wittekindt, O.H., Frick, M., and Philipp, M. (2019).
989 Pharmacological cholesterol depletion disturbs ciliogenesis and ciliary function in developing
990 zebrafish. Communications Biology 1–13.

991 Martens, G.W., Arikan, M.C., Lee, J., Ren, F., Vallerskog, T., and Kornfeld, H. (2008).
992 Hypercholesterolemia Impairs Immunity to Tuberculosis. Infection and Immunity *76*, 3464–
993 3472.

994 Medzhitov, R. (2007). Recognition of microorganisms and activation of the immune response.
995 Nature *449*, 819–826.

996 Moliva, J.I., Hossfeld, A.P., Sidiki, S., Canan, C.H., Dwivedi, V., Beamer, G., Turner, J., and
997 Torrelles, J.B. (2019). Selective delipidation of Mycobacterium bovis BCG enables direct
998 pulmonary vaccination and enhances protection against Mycobacterium tuberculosis. Mucosal
999 Immunology *12*, 805–815.

1000 Murry, J.P., Pandey, A.K., Sassetti, C.M., and Rubin, E.J. (2009). Phthiocerol dimycocerosate
1001 transport is required for resisting interferon-gamma-independent immunity. J Infect Dis *200*,
1002 774–782.

1003 Nishijima, K., Yoneda, M., Hirai, T., Takakuwa, K., and Enomoto, T. (2019). Biology of the
1004 vernix caseosa: A review. J. Obstet. Gynaecol. Res. *45*, 2145–2149.

1005 Onwueme, K.C., Vos, C.J., Zurita, J., Ferreras, J.A., and Quadri, L.E.N. (2005). The
1006 dimycocerosate ester polyketide virulence factors of mycobacteria. Progress in Lipid Research
1007 *44*, 259–302.

1008 Osman, M.M., Pagán, A.J., Shanahan, J.K., and Ramakrishnan, L. (2020). Mycobacterium
1009 marinumphthiocerol dimycocerosates enhance macrophage phagosomal permeabilization and
1010 membrane damage. bioRxiv 1–20.

1011 Pandey, A.K., and Sassetti, C.M. (2008). Mycobacterial persistence requires the utilization of
1012 host cholesterol. Proceedings of the National Academy of Sciences *105*, 4376–4380.

1013 Poger, D., Caron, B., and Mark, A.E. (2014). Effect of Methyl-Branched Fatty Acids on the
1014 Structure of Lipid Bilayers. J. Phys. Chem. B *118*, 13838–13848.

1015 Quigley, J., Hughitt, V.K., Velikovsky, C.A., Mariuzza, R.A., El-Sayed, N.M., and Briken, V.
1016 (2017). The Cell Wall Lipid PDIM Contributes to Phagosomal Escape and Host Cell Exit of
1017 Mycobacterium tuberculosis. mBio *8*, e00148–17–12.

1018 Ramakrishnan, L. (2012). Revisiting the role of the granuloma in tuberculosis. Nat Rev Immunol
1019 *12*, 352–366.

1020 Ramakrishnan, L. (2020). Mycobacterium tuberculosis pathogenicity viewed through the lens of
1021 molecular Koch's postulates. Curr. Opin. Microbiol. *54*, 103–110.

1022 Ran-Ressler, R.R., Khailova, L., Arganbright, K.M., Adkins-Rieck, C.K., Jouni, Z.E., Koren, O.,
1023 Ley, R.E., Brenna, J.T., and Dvorak, B. (2011). Branched Chain Fatty Acids Reduce the
1024 Incidence of Necrotizing Enterocolitis and Alter Gastrointestinal Microbial Ecology in a
1025 Neonatal Rat Model. PLoS ONE *6*, e29032–10.

1026 Reuschl, A.-K., Edwards, M.R., Parker, R., Connell, D.W., Hoang, L., Halliday, A., Jarvis, H.,
1027 Siddiqui, N., Wright, C., Bremang, S., et al. (2017). Innate activation of human primary
1028 epithelial cells broadens the host response to Mycobacterium tuberculosis in the airways. PLoS
1029 Pathog *13*, e1006577–26.

1030 Rodriguez-Rivera, F.P., Zhou, X., Theriot, J.A., and Bertozzi, C.R. (2017). Visualization of
1031 mycobacterial membrane dynamics in live cells. J. Am. Chem. Soc. *139*, 3488–3495.

1032 Rousseau, C., Winter, N., Pivert, E., Bordat, Y., Neyrolles, O., Avé, P., Huerre, M., Gicquel, B.,
1033 and Jackson, M. (2004). Production of phthiocerol dimycocerosates protects Mycobacterium
1034 tuberculosis from the cidal activity of reactive nitrogen intermediates produced by macrophages
1035 and modulates the early immune response to infection. Cellular Microbiology *6*, 277–287.

1036 Ruysschaert, J.-M., and Lonez, C. (2015). Role of lipid microdomains in TLR-mediated
1037 signalling. BBA - Biomembranes *1848*, 1860–1867.

1038 Siegrist, M.S., Swarts, B.M., Fox, D.M., Lim, S.A., and Bertozzi, C.R. (2015). Illumination of
1039 growth, division and secretion by metabolic labeling of the bacterial cell surface. FEMS
1040 Microbiology Reviews *39*, 184–202.

1041 Silva, C.L., Ekizlerian, S.M., and Fazioli, R.A. (1985). Role of cord factor in the modulation of
1042 infection caused by mycobacteria. Am. J. Pathol. *118*, 238–247.

1043 Siméone, R., Constant, P., Malaga, W., Guilhot, C., Daffé, M., and Chalut, C. (2007). Molecular
1044 dissection of the biosynthetic relationship between phthiocerol and phthiodiolone
1045 dimycocerosates and their critical role in the virulence and permeability of Mycobacterium
1046 tuberculosis. FEBS Journal *274*, 1957–1969.

1047 Sletten, E.M., and Bertozzi, C.R. (2009). Bioorthogonal chemistry: fishing for selectivity in a sea
1048 of functionality. Angew. Chem. Int. Ed. Engl. *48*, 6974–6998.

1049 Soh, A.Z., Chee, C.B., Wang, Y.-T., Yuan, J.-M., and Koh, W.-P. (2016). Dietary Cholesterol
1050 Increases the Risk whereas PUFAs Reduce the Risk of Active Tuberculosis in Singapore
1051 Chinese. The Journal of Nutrition *146*, 1093–1100.

1052 Soong, G., Reddy, B., Sokol, S., Adamo, R., and Prince, A. (2004). TLR2 is mobilized into an
1053 apical lipid raft receptor complex to signal infection in airway epithelial cells. J. Clin. Invest.
1054 *113*, 1482–1489.

1055 Srivastava, S., Ernst, J.D., and Desvignes, L. (2014). Beyond macrophages: the diversity of
1056 mononuclear cells in tuberculosis. Immunol. Rev. *262*, 179–192.

1057 Swarts, B.M., Holsclaw, C.M., Jewett, J.C., Alber, M., Fox, D.M., Siegrist, M.S., Leary, J.A.,
1058 Kalscheuer, R., and Bertozzi, C.R. (2012). Probing the mycobacterial trehalome with
1059 bioorthogonal chemistry. J. Am. Chem. Soc. *134*, 16123–16126.

1060 Takaki, K., Davis, J.M., Winglee, K., and Ramakrishnan, L. (2013). Evaluation of the
1061 pathogenesis and treatment of Mycobacterium marinum infection in zebrafish. Nat Protoc *8*,
1062 1114–1124.

1063 Tall, A.R., and Yvan-Charvet, L. (2015). Cholesterol, inflammation and innate immunity. Nature
1064 Publishing Group 1–13.

1065 Urbanek, B.L., Wing, D.C., Haislop, K.S., Hamel, C.J., Kalscheuer, R., Woodruff, P.J., and
1066 Swarts, B.M. (2014). Chemoenzymatic Synthesis of Trehalose Analogues: Rapid Access to
1067 Chemical Probes for Investigating Mycobacteria. Chembiochem *15*, 2066–2070.

1068 Urdahl, K.B. (2014). Understanding and overcoming the barriers to T cell-mediated immunity
1069 against tuberculosis. Seminars in Immunology *26*, 578–587.

1070 van der Wel, N., Hava, D., Houben, D., Fluitsma, D., van Zon, M., Pierson, J., Brenner, M., and
1071 Peters, P.J. (2007). M. tuberculosis and M. leprae translocate from the phagolysosome to the
1072 cytosol in myeloid cells. Cell *129*, 1287–1298.

1073 Volkman, H.E., Pozos, T.C., Zheng, J., Davis, J.M., Rawls, J.F., and Ramakrishnan, L. (2010).
1074 Tuberculous Granuloma Induction via Interaction of a Bacterial Secreted Protein with Host
1075 Epithelium. Science *327*, 466–469.

1076 Walton, E.M., Cronan, M.R., Beerman, R.W., and Tobin, D.M. (2015). The Macrophage-
1077 Specific Promoter mfap4 Allows Live, Long-Term Analysis of Macrophage Behavior during
1078 Mycobacterial Infection in Zebrafish. PLoS ONE *10*, e0138949.

1079 Wells, W.F., Ratcliffe, H.L., and Grumb, C. (1948). On the mechanics of droplet nuclei
1080 infection; quantitative experimental air-borne tuberculosis in rabbits. Am J Hyg *47*, 11–28.

1081

1082

1083

1084 **Supplemental Figures, Movie, and Table**

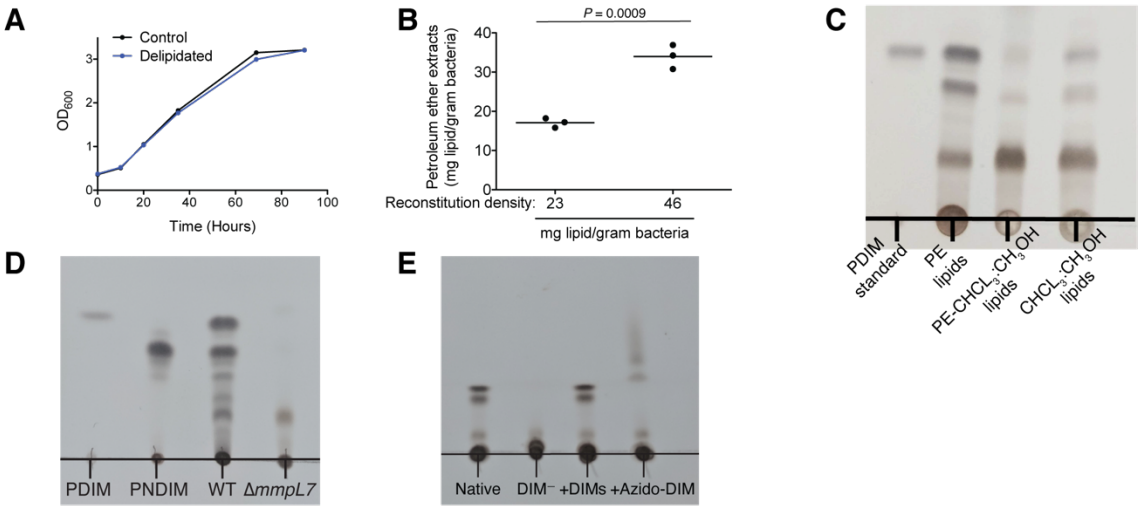

Supplemental Figure 1. Optimization of petroleum ether extraction and reconstitution. (**A**) Mean OD_{600} values of control or delipidated *M. marinum* recovered in complete growth medium. (**B**) Mean mg of lipid extracted per gram of dry bacteria following reconstitution with designated lipid densities. Two-tailed, unpaired t test. (**C**) Thin-layer chromatography (TLC) showing PDIM's complete removal following petroleum ether extraction. PDIM standard, petroleum ether extract (PE lipids), chloroform:methanol extract of the bacterial pellet previously extracted with petroleum ether (PE-CHCL3:CH3OH lipids), and chloroform:methanol extract of a fresh bacterial pellet (CHCL3:CH3OH lipids). TLC was ran twice in 98:2 petroleum ether:ethyl acetate. (**D**) TLC of PDIM standard, PNDIM standard, and petroleum ether extracts of wildtype (WT) and Δ*mmpL7 M. marinum*. TLC was ran twice in 98:2 petroleum ether:ethyl acetate. (**E**) TLC of Native, DIM depleted (DIM^-), DIM^- plus native DIMs (+DIMs), or DIM^- plus azido-DIM (+Azido-DIM) lipids prior to reconstitution onto delipidated bacteria. TLC was ran once in 98:2 petroleum ether:ethyl acetate. (**A**)-(**E**) representative of three separate experiments.

1085
1086
1087
1088
1089
1090
1091
1092
1093
1094
1095
1096
1097
1098
1099

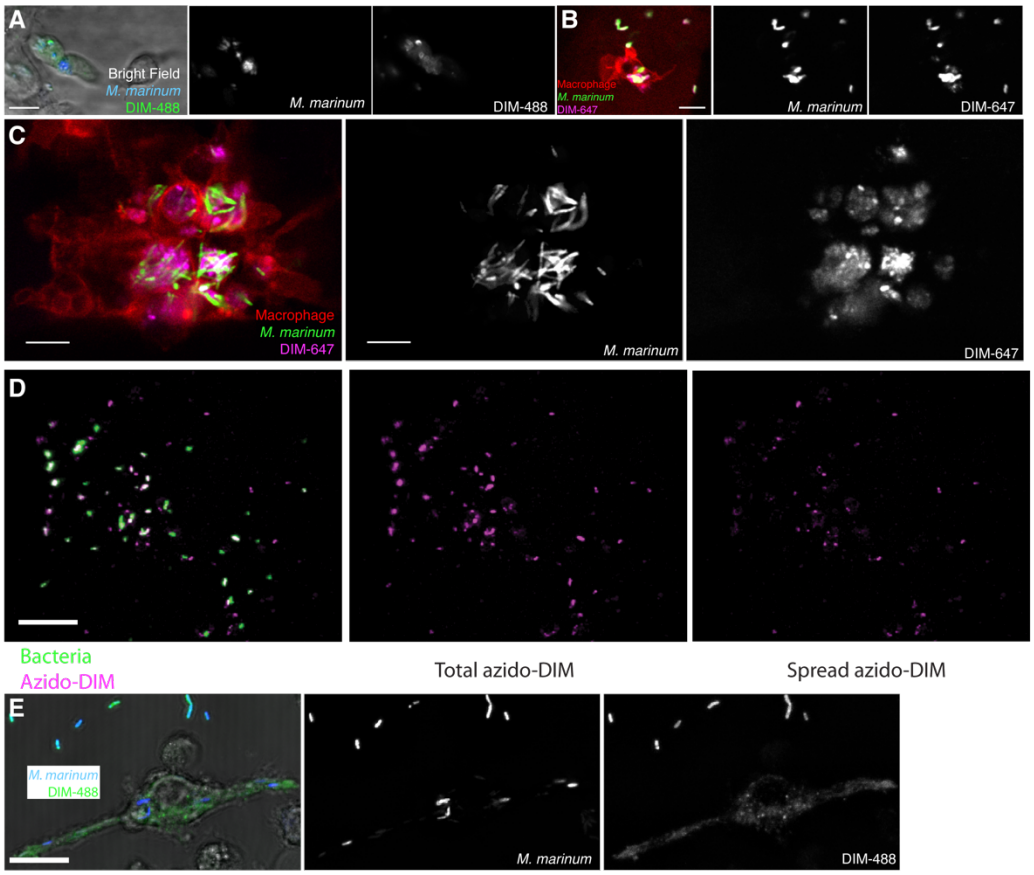

Supplemental Figure 2. Further characterization of PDIM spread**.** (**A**) Image of *M. marinum* expressing a cytosolic blue fluorescent protein reconstituted with DIBO-488 (green) labeled azido-DIM at 3hpi of ~100 *M. marinum* in the HBV of wildtype fish. Scale bar = 10μm. Images of *M. marinum* expresisng a cytosolic wasabi flourescent protein reconstituted with DIBO-647 labelled azido-DIM (DIM-647) at (**B**) 3 hours post infection and (**C**) 3 days post infection of ~100 *M. marinum* in the HBV of transgenic fish whose macrophages express the red flourescent protein tdTomato. Scale bar = 10μm. (**D**) Example of calculating percent spread: A surface rendering of the cytosolic expressing protein of the flourescent bacteria (green) is subtracted from the total azido-DIM signal (magenta) to give the spread azido-DIM signal. The volume of the spread azido-DIM signal is then divided by the volume of the total azido-DIM signal to calculate percent spread. Scale bar = 50μm. (**E**) Image of *M. marinum* expresisng a blue fluorescent protein reconstituted with DIM-488 24 hpi of THP-1 macrophages, MOI = 5, and scale bar = 10μm.

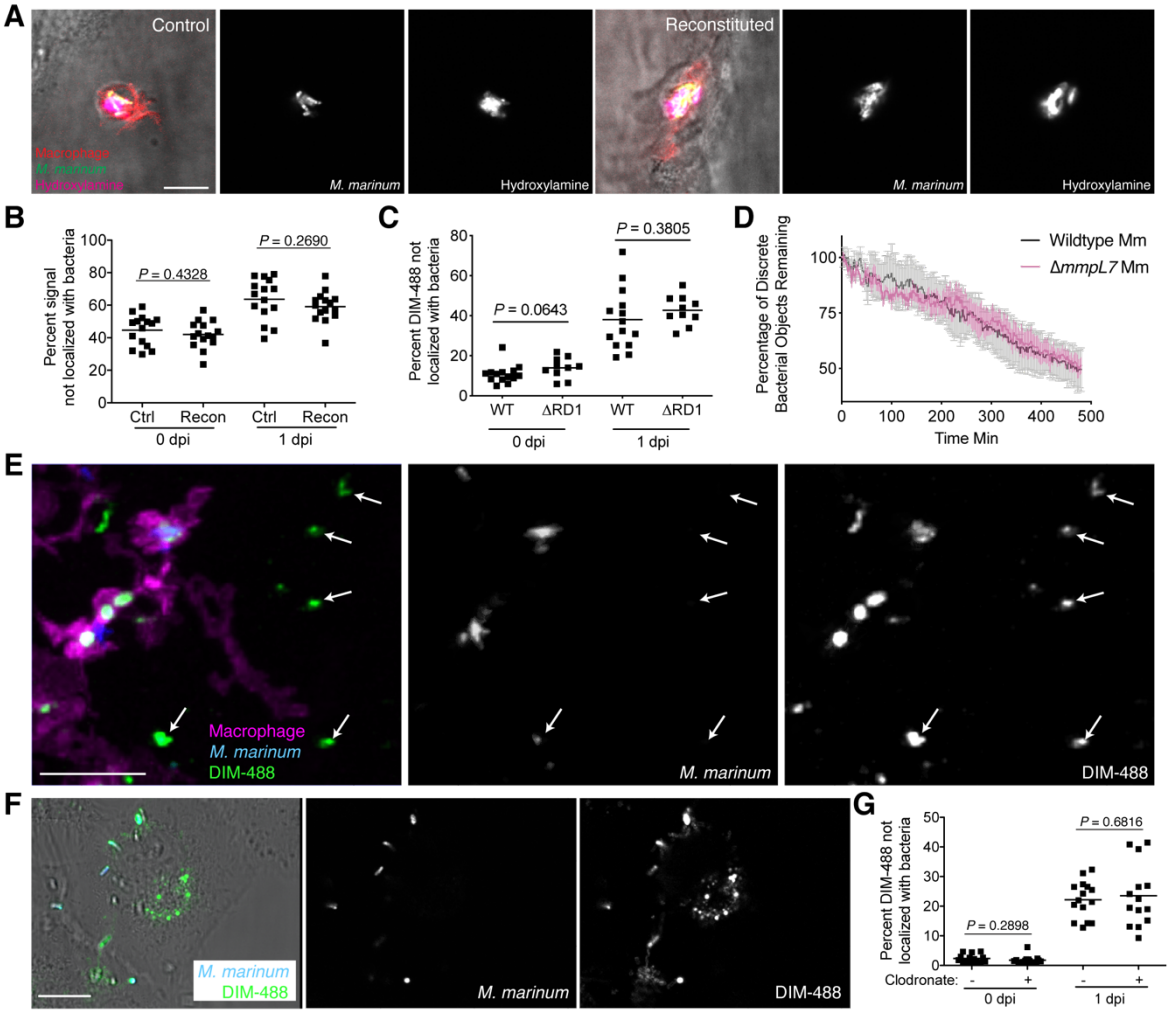

Supplemental Figure 3. Functional evaluation of PDIM spread. (**A**) Images of control or reconstituted *M. marinum* expressing a cytosolic green fluorescent protein labeled with periodate-hydroxylamine chemistry at 3 hpi of ~100 *M. marinum* into the HBV of transgenic fish whose macrophages express a fluorescent protein, scale bar = 10μm. (**B**) Mean percent fluorescent signal not localized with bacteria following HBV infection of wildtype fish with ~100 control or reconstituted *M. marinum* labeled with periodate-hydroxylamine chemistry. Two-tailed, unpaired t test. (**C**) Mean percent DIM-488 not localized with bacteria following HBV infection of wildtype fish with ~100 wildtype or ΔRD1 *M. marinum*. Two-tailed Mann Whitney test for 0 dpi and two-tailed, unpaired t test for 1 dpi (**D**) Mean (+/- SEM) percentage of discrete bacterial objects remaining following HBV infection of wildtype fish with ~100 wildtype or Δ*mmpL7 M. marinum*. Representative of two separate experiments. (**E**) Image of *M. marinum* expressing a cytosolic blue fluorescent protein reconstituted with DIBO-488 labeled azido-DIM (DIM-488) highlighting DIM-488 spread on epithelial cells (arrows) at 24 hpi of ~100 *M. marinum* in the HBV of transgenic fish whose macrophages express a fluorescent protein, scale bar = 30μm. (**F**) Image of *M. marinum* expressing a blue fluorescent protein reconstituted with DIM-488 24 hpi of A549 epithelial cells at an MOI of 5, scale bar = 10μm. (**G**) Mean percent DIM-488 not localized with bacteria following HBV infection of lipo-PBS or lipo-clodronate treated fish with ~100 *M. marinum*. Two-tailed Mann Whitney test for 0 dpi and two-tailed, unpaired t test for 1 dpi. (B), (C), and (G) representative of three separate experiments.

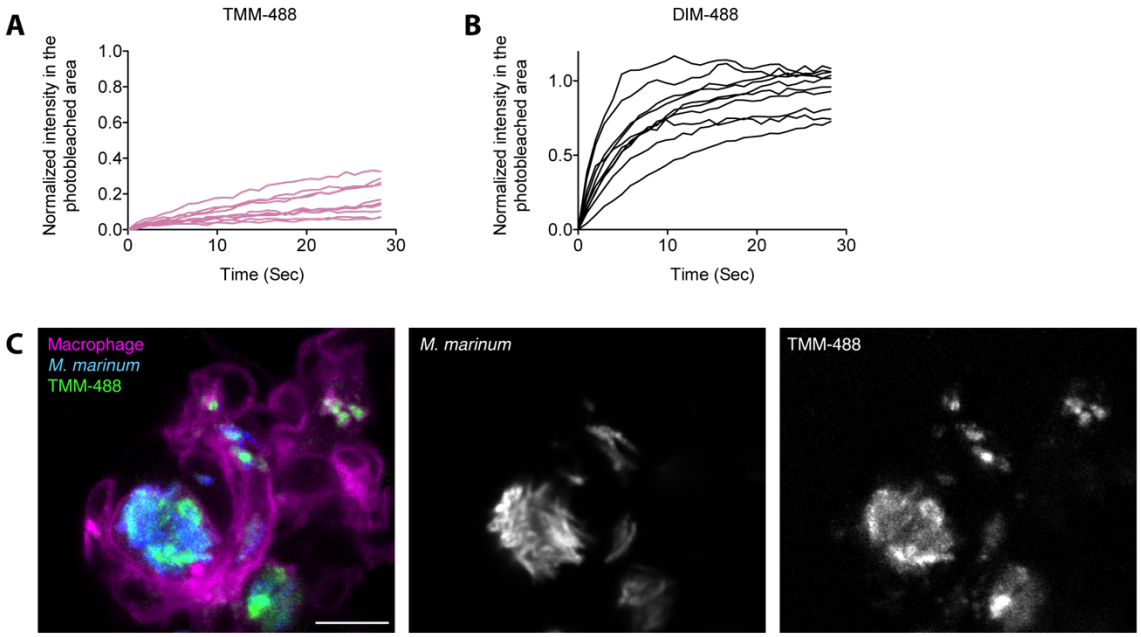

Supplemental Figure 4. Individual FRAP curves of (**A**) TMM-488 and (**B**) DIM-488 labeled bacteria. (**C**) Image of *M. marinum* expressing a cytosolic blue fluorescent protein metabolically labeled with 6-azido trehalose followed by labeling with DIBO-488 (TMM-488) highlighting TMM-488 spread across macrophage membranes at 24 hpi of ~100 *M. marinum* in the HBV of transgenic fish whose macrophages express a fluorescent protein.

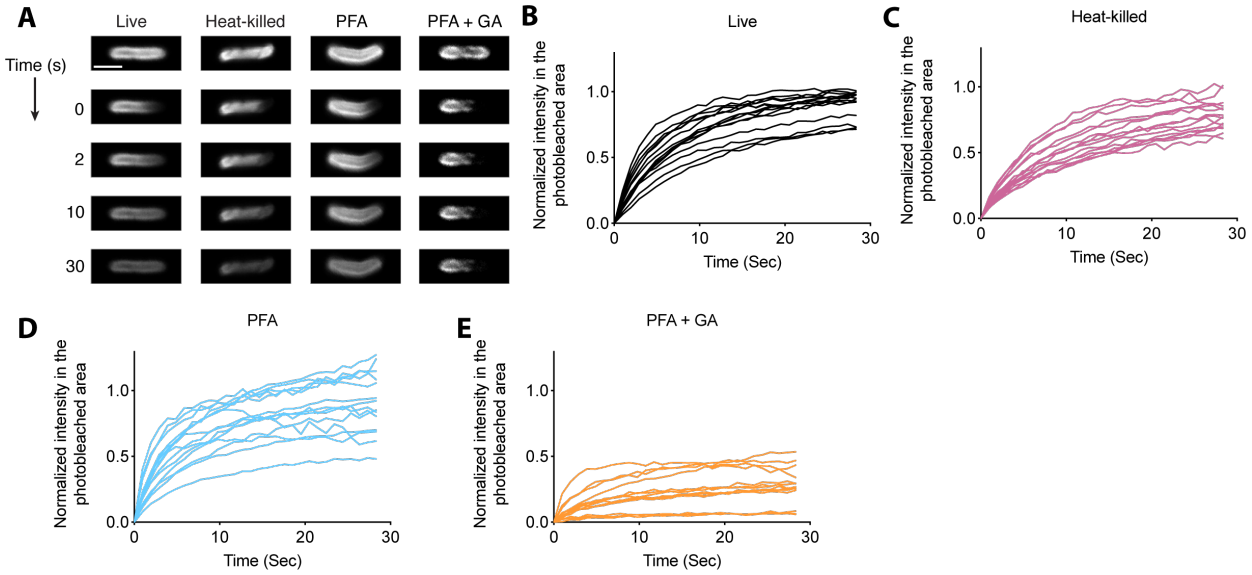

Supplemental Figure 5. FRAP analysis of DIM-488 labeled bacteria. (**A**) Representative FRAP images of live, heat-killed, PFA, and PFA+GA treated DIM-488 labeled *M. marinum*, scale bar = 2μm. (**B**-**E**) Individual fluorescent recovery curves of bacteria described in **A**. Representative of three separate experiments.

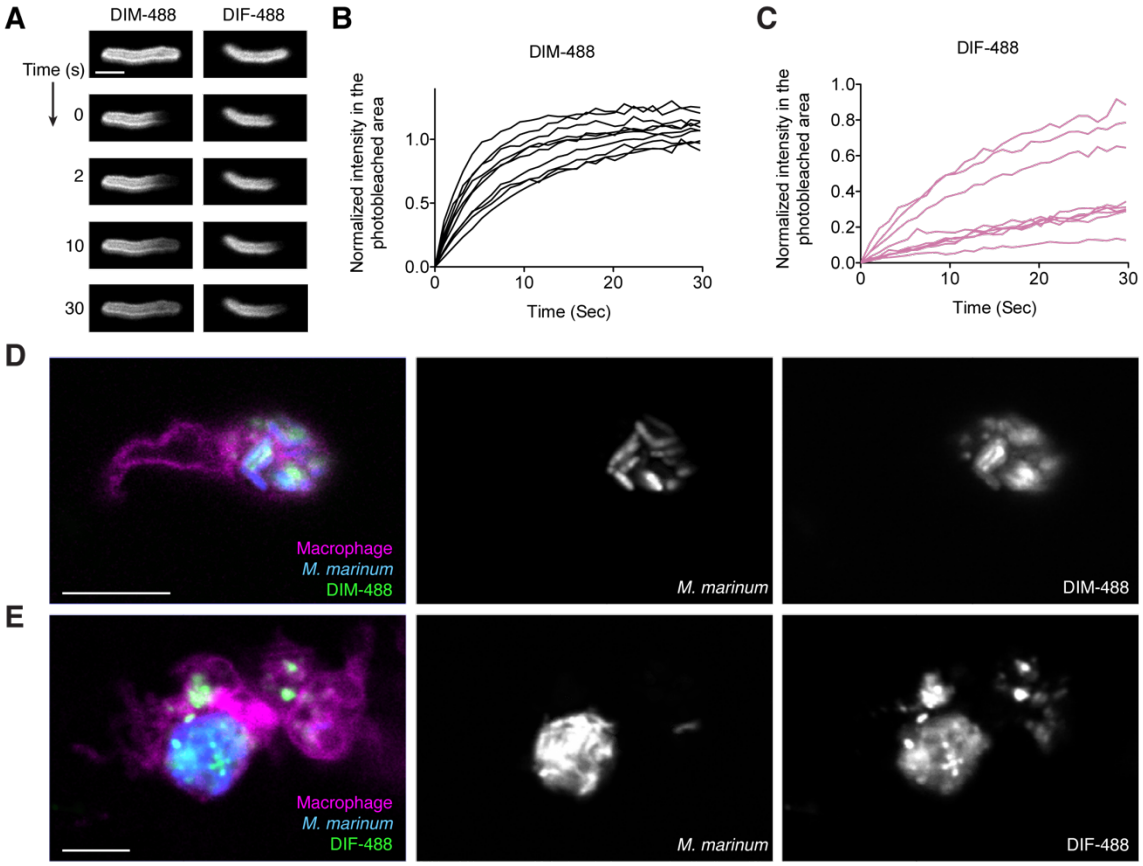

Supplementary Figure 6. Analysis of DIM-488 and DIF-488 labeled *M. marinum*. (**A**) Representative FRAP images of DIM-488 and DIF-488 labeled *M. marinum*, scale bar = 2*µ*m. Individual fluorescent recovery curves of (**B**) DIM-488 and (**C**) DIF-488 labeled *M. marinum*. Images of *M. marinum* expressing a cytosolic blue fluorescent protein reconstituted with green (**D**) DIM-488 or (**E**) DIF-488 at 24hpi of ~100 *M. marinum* in the HBV of transgenic fish whose macrophages express a red fluorescent protein. Scale bar = 10µm. (**B**) and (**C**) represenatative of three separate experiments.

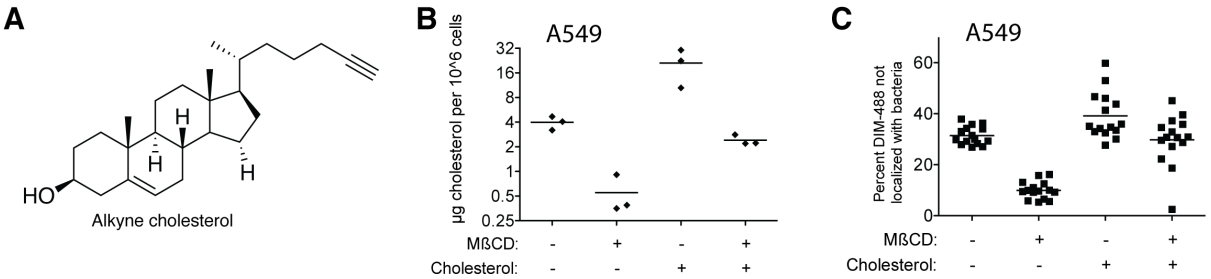

Supplementary Figure 7. Cholesterol mediates DIM-488 spread on A549 epithelial cells. (**A**) Structure of alkyne cholesterol. (**B**) Mean cholesterol content of A549 cells treated with methyl-ß cyclodextrin (MßCD), water-soluble cholesterol, or both. (**C**) Mean percent DIM-488 spread at 24 hpi of A549 epithelial cells treated with MßCD, water-soluble cholesterol, or both, MOI = 5. (**B**) and (**C**) representative of three separate experiments.

1187 **Movie S1: PDIM dynamics**. Real-time video of *M. marinum* expressing blue fluorescent protein
1188 reconstituted with DIBO-488 labelled azido-DIM at 3 hpi of the HBV with ~100 *M. marinum*.
1189
1190 **Supplementary Table 1**. Summary of *P* values and statistical tests. Gaussian distribution was
1191 determined using the D'Agostino-Pearson normality test. The result of this test guided
1192 subsequent analyses.
1193
1194
1195
1196
1197
1198
1199
1200
1201
1202
1203
1204
1205
1206
1207
1208
1209
1210
1211
1212
1213
1214
1215
1216
1217

NMR SPECTRA

^{1}H NMR

500 MHz

$CDCl_3$

PDIM

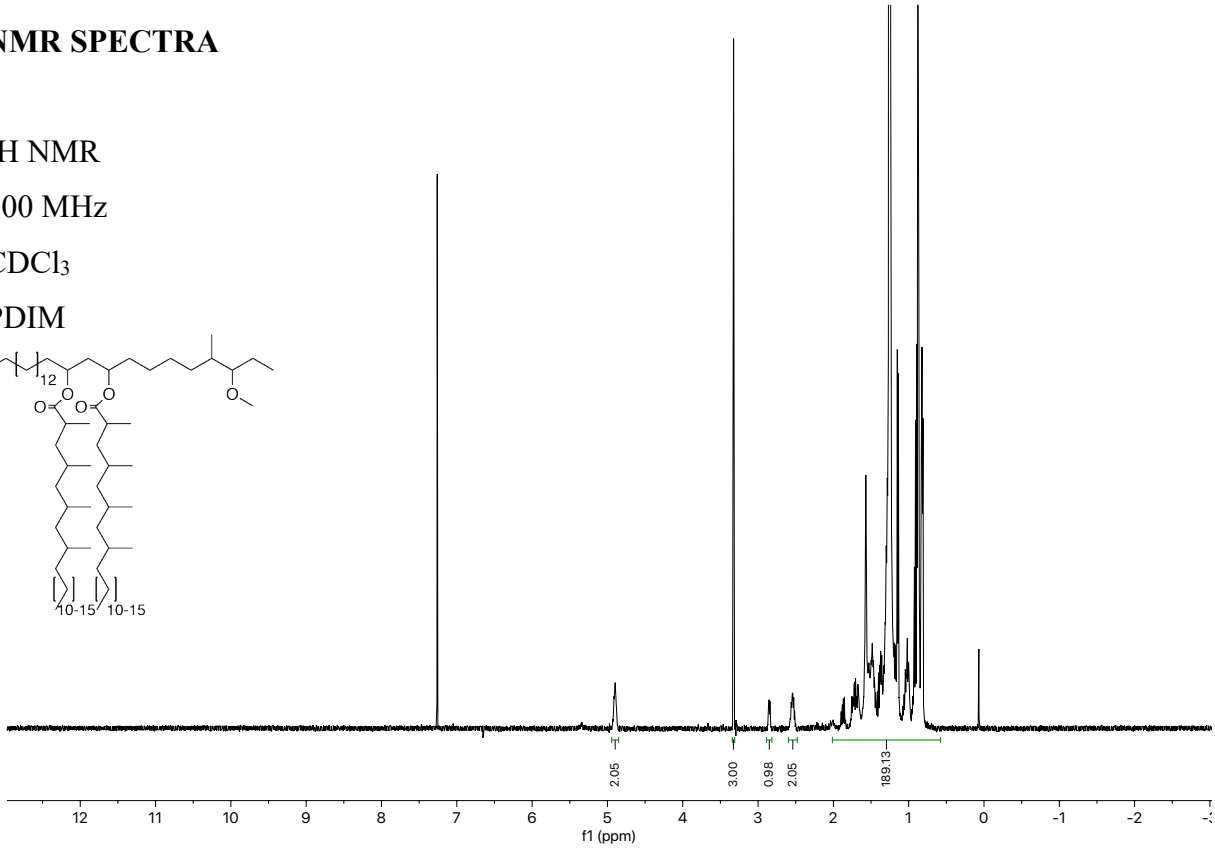

^{13}C NMR

126 MHz

$CDCl_3$

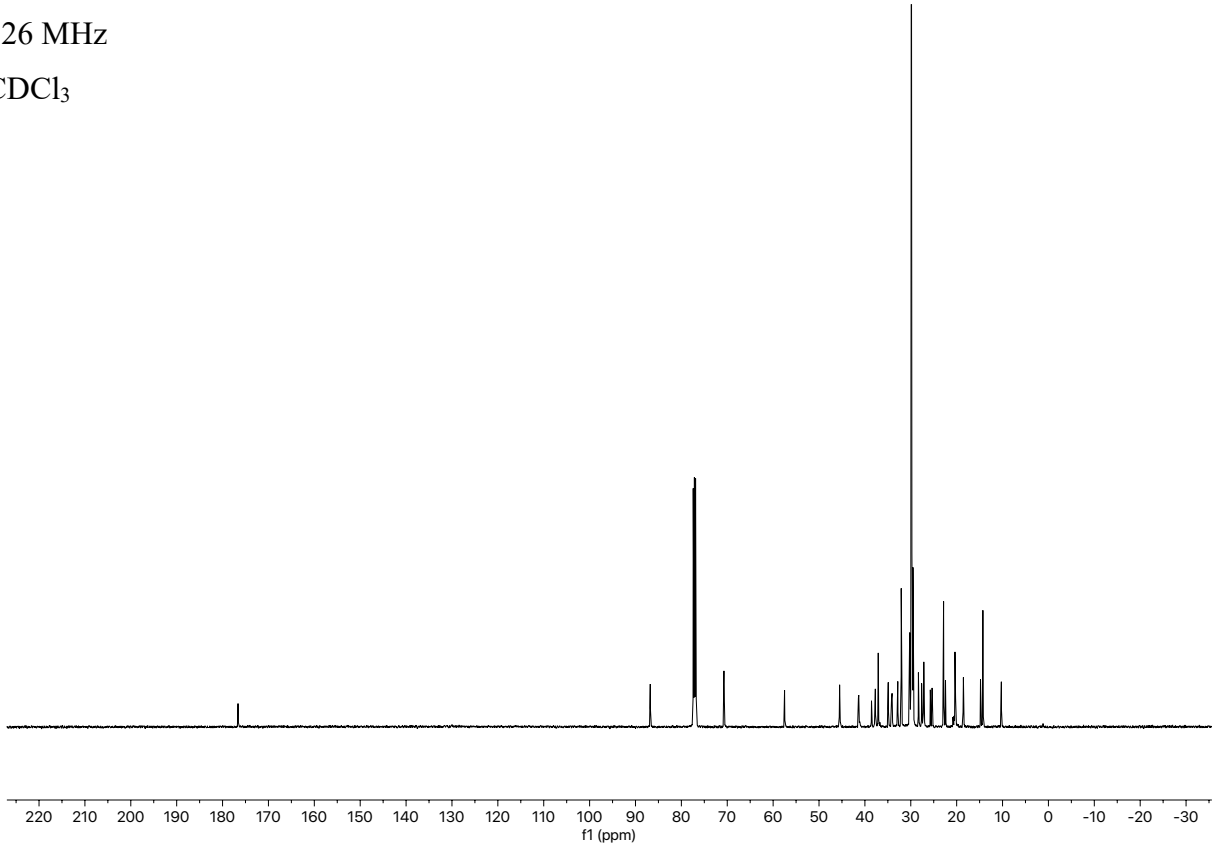

^{1}H NMR

500 MHz

$CDCl_3$

Azido-DIM

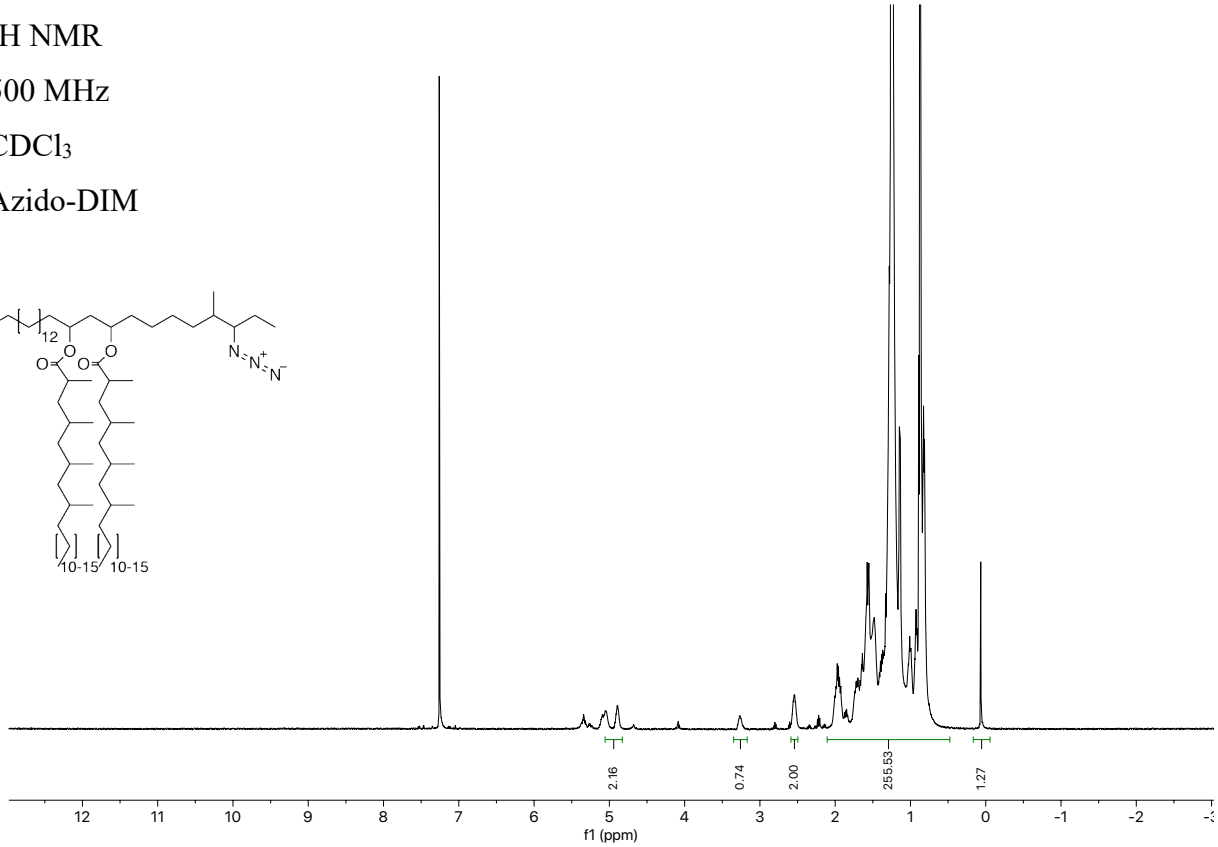

^{13}C NMR

126 MHz

$CDCl_3$

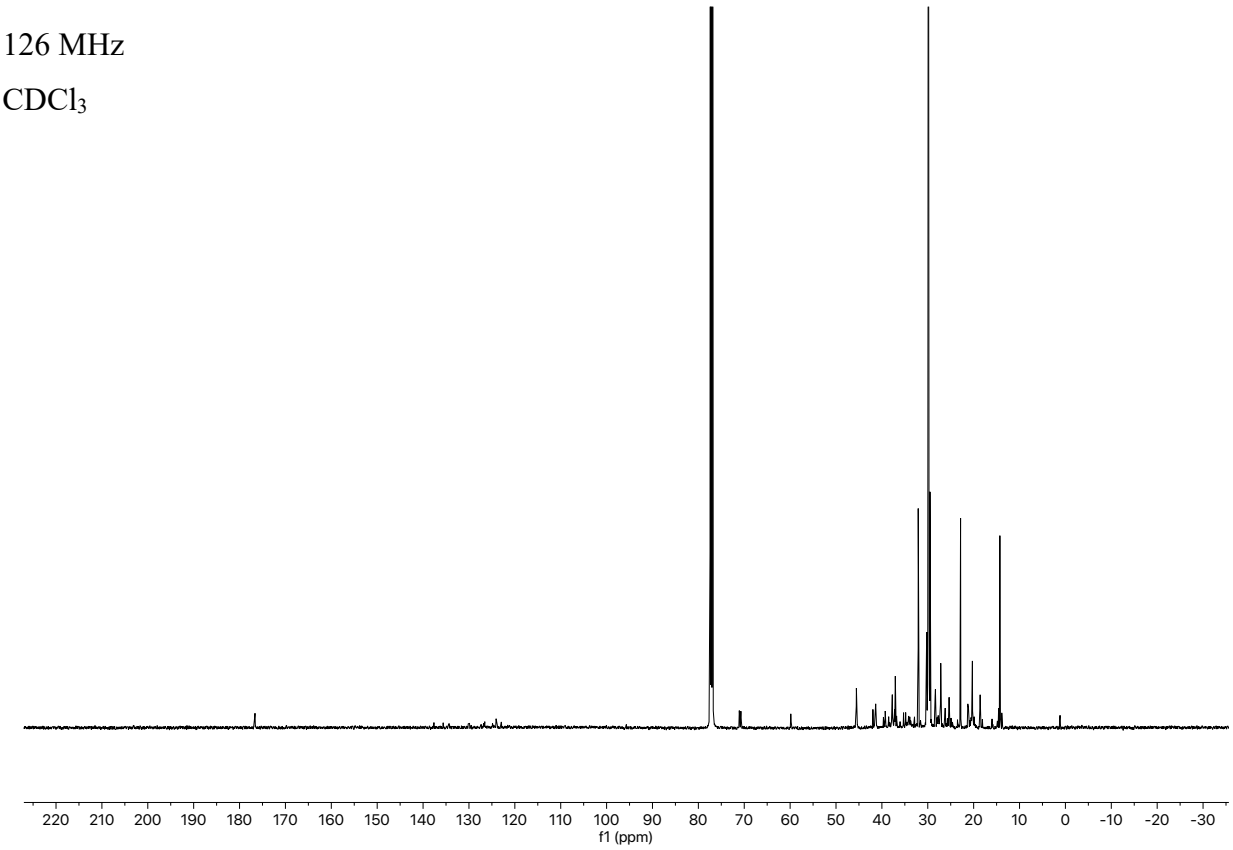

^{1}H NMR

500 MHz

$CDCl_3$

PDIF

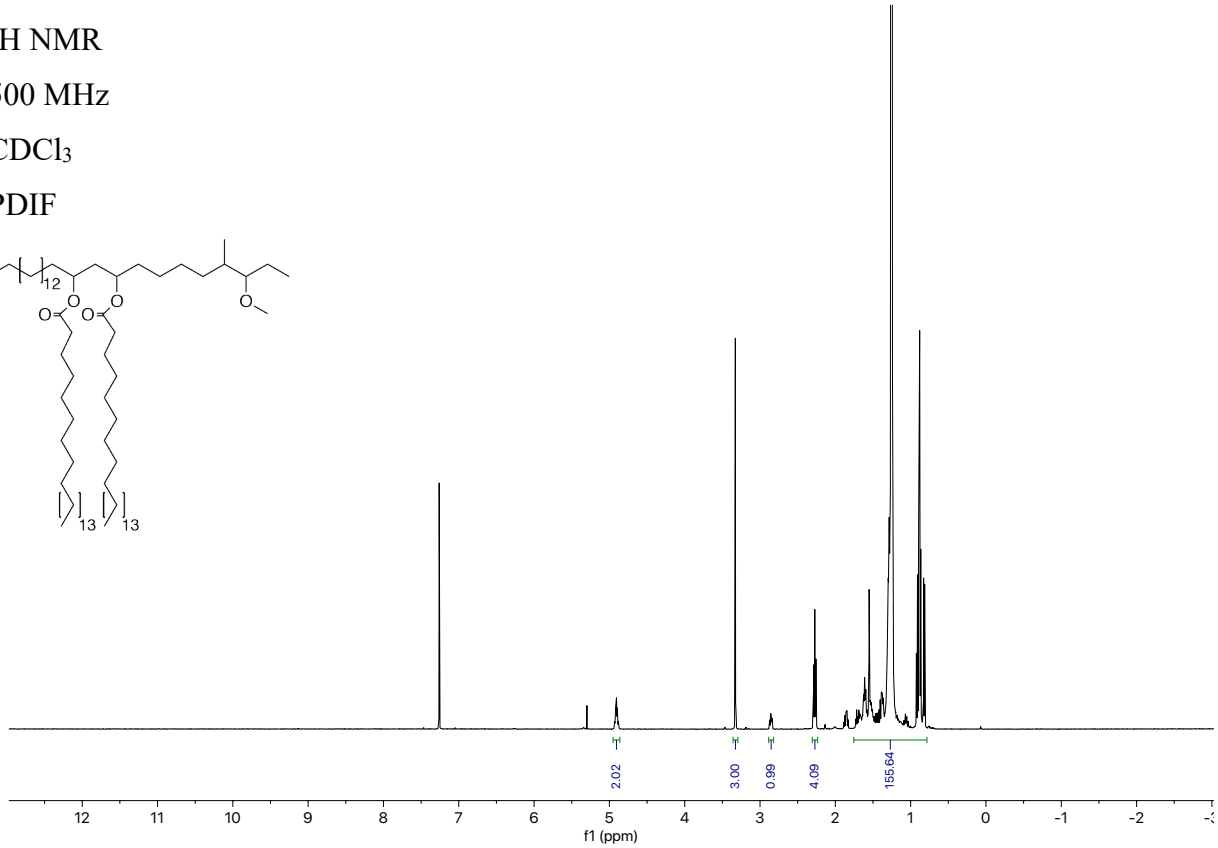

^{13}C NMR

126 MHz

$CDCl_3$

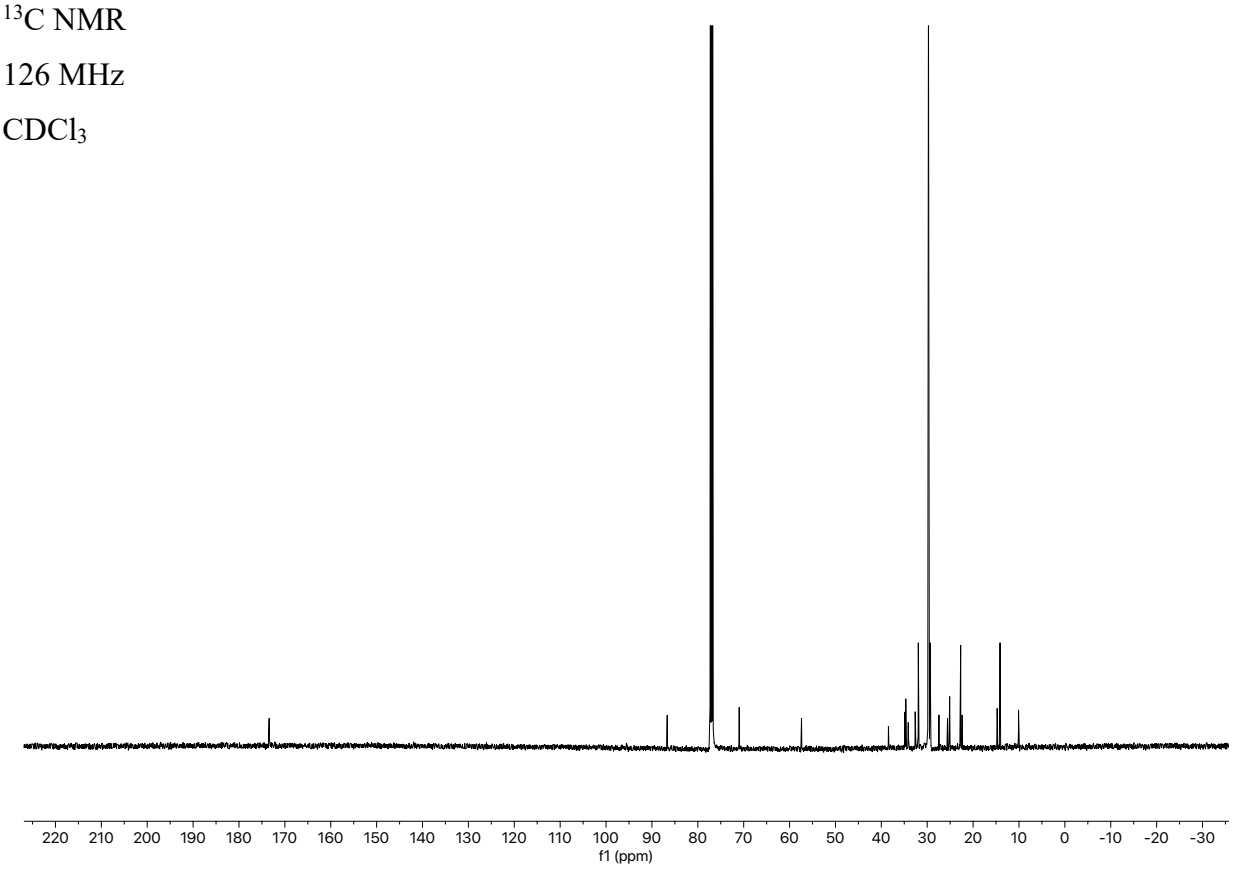

^{1}H NMR

500 MHz

$CDCl_3$

Azido-DIF

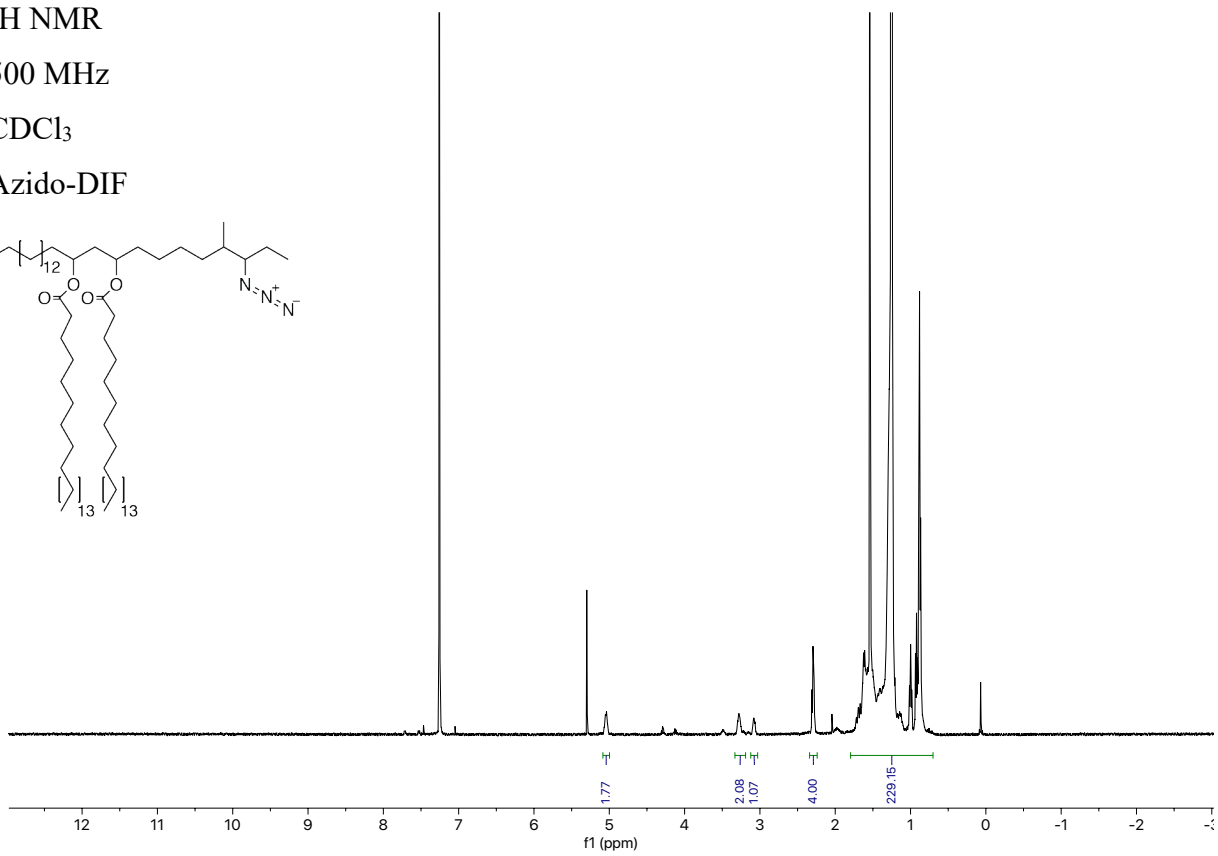

^{13}C NMR

126 MHz
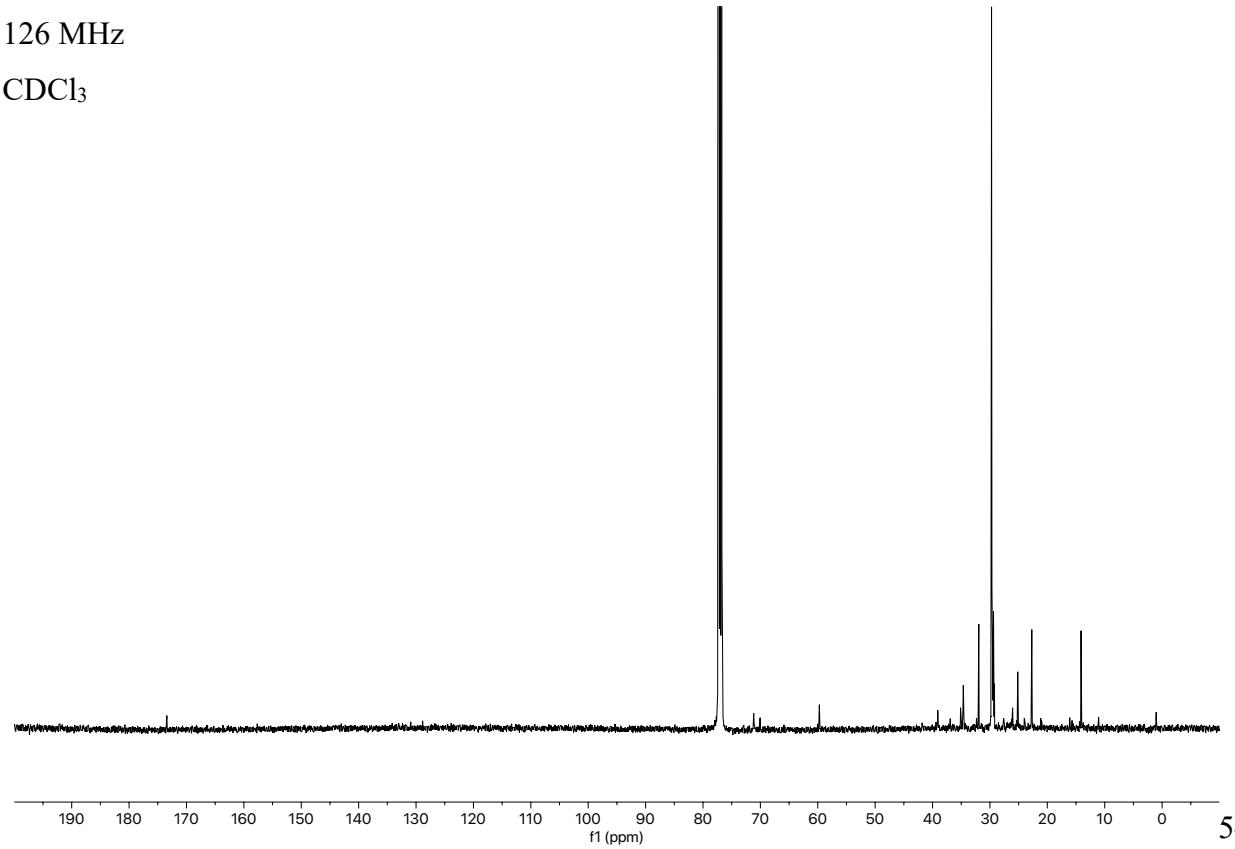
$CDCl_3$